AFRL-RX-WP-JA-2020-0244

EMERGING APPLICATIONS OF ELEMENTAL 2D MATERIALS (POSTPRINT)

Nicholas R. Glavin, Vikas Varshney, and Ajit Roy

AFRL/RXAS

Rahul Rao

UES, Incorporated

29 July 2019
Interim Report

(STINFO COPY)

AIR FORCE RESEARCH LABORATORY
MATERIALS AND MANUFACTURING DIRECTORATE
WRIGHT-PATTERSON AIR FORCE BASE, OH 45433-7750
AIR FORCE MATERIEL COMMAND
UNITED STATES AIR FORCE

REPORT DOCUMENTATION PAGE

Form Approved
OMB No. 0704-0188

1. REPORT DATE *(DD-MM-YY)*	2. REPORT TYPE	3. DATES COVERED *(From - To)*
29 July 2019	Interim	29 December 2018 - 29 June 2019

4. TITLE AND SUBTITLE
Emerging Applications of Elemental 2D Materials (Postprint)

5a. CONTRACT NUMBER
In-House

5b. GRANT NUMBER

5c. PROGRAM ELEMENT NUMBER

6. AUTHOR(S)
Nicholas R. Glavin, Vikas Varshney and Ajit Roy – AFRL/RXAS

(Continued on next page)

5d. PROJECT NUMBER

5e. TASK NUMBER

5f. WORK UNIT NUMBER
X1SQ

7. PERFORMING ORGANIZATION NAME(S) AND ADDRESS(ES)
AFRL/RX
2977 Hobson Way (Continued on next page)
Wright-Patterson AFB OH 45433

8. PERFORMING ORGANIZATION REPORT NUMBER
1)

9. SPONSORING/MONITORING AGENCY NAME(S) AND ADDRESS(ES)
Air Force Research Laboratory
Materials and Manufacturing Directorate
Wright-Patterson Air Force Base, OH 45433-7750
Air Force Materiel Command
United States Air Force

10. SPONSORING/MONITORING AGENCY ACRONYM(S)
AFRL/RXAS

11. SPONSORING/MONITORING AGENCY REPORT NUMBER(S)
AFRL-RX-WP-JA-2020-0244

12. DISTRIBUTION/AVAILABILITY STATEMENT
DISTRIBUTION STATEMENT A. Approved for public release: distribution is unlimited.

13. SUPPLEMENTARY NOTES
PA Case Number: 88ABW-2019-2970; Clearance Date: 13 June 2019. This document contains color. Journal article published in Advanced Materials, Vol. 32, No. 7, online 31 Oct 2019, published 20 Feb 2020. The U.S. Government is joint author of the work and has the right to use, modify, reproduce, release, perform, display, or disclose the work. The final publication is available at https://doi-org.wrs.idm.oclc.org/10.1002/adma.201904302

14. ABSTRACT ***(Maximum 200 words)***
As elemental main group materials (i.e., silicon and germanium) have dominated the field of modern electronics, their monolayer 2D analogues have shown great promise for next-generation electronic materials as well as potential game-changing properties for optoelectronics, energy, and beyond. These atomically thin materials composed of single atomic variants of group III through group VI elements on the periodic table have already demonstrated exciting properties such as near-room-temperature topological insulation in bismuthene, extremely high electron mobilities in phosphorene and silicone, and substantial Li-ion storage capability in borophene. Isolation of these materials within the postgraphene era began with silicene in 2010 and quickly progressed to the experimental identification or theoretical prediction of 15 of the 18 main group elements existing as solids at standard pressure and temperatures. This review first focuses on the significance of defects/functionalization, discussion of different allotropes, and overarching structure–property relationships of 2D main group elemental materials.

15. SUBJECT TERMS
Monolayer 2D analogues, optoelectronics, topological insulation, bismuthene, phosphorene, silicone, allotropes,

16. SECURITY CLASSIFICATION OF:			17. LIMITATION OF ABSTRACT:	18. NUMBER OF PAGES	19a. NAME OF RESPONSIBLE PERSON (Monitor)
a. REPORT	b. ABSTRACT	c. THIS PAGE			Marc Martin
Unclassified	Unclassified	Unclassified	SAR	25	19b. TELEPHONE NUMBER *(Include Area Code)* (937) 255-9645

β-Ga_2O_3REPORT DOCUMENTATION PAGE Cont'd

6. AUTHOR(S)

Nicholas R. Glavin, Vikas Varshney, and Ajit Roy - AFRL/RXAS

Rahul Rao - UES, Inc.

Elisabeth Bianco, Amey Apte, Emillie Ringe and Pulickel Ajayan - Rice University

7. PERFORMING ORGANIZATION NAME(S) AND ADDRESS(ES)

AFRL/RX
2977 Hobson Way
Wright-Patterson AFB OH 45433

UES, Incorporated
4401 Dayton Xenia Road
Beavercreek OH 45432

Rice University
6100 Main St
Houston TX 77005

ADVANCED MATERIALS
www.advmat.de

Emerging Applications of Elemental 2D Materials

Nicholas R. Glavin, Rahul Rao, Vikas Varshney, Elisabeth Bianco, Amey Apte, Ajit Roy, Emilie Ringe, and Pulickel M. Ajayan**

As elemental main group materials (i.e., silicon and germanium) have dominated the field of modern electronics, their monolayer 2D analogues have shown great promise for next-generation electronic materials as well as potential game-changing properties for optoelectronics, energy, and beyond. These atomically thin materials composed of single atomic variants of group III through group VI elements on the periodic table have already demonstrated exciting properties such as near-room-temperature topological insulation in bismuthene, extremely high electron mobilities in phosphorene and silicone, and substantial Li-ion storage capability in borophene. Isolation of these materials within the postgraphene era began with silicene in 2010 and quickly progressed to the experimental identification or theoretical prediction of 15 of the 18 main group elements existing as solids at standard pressure and temperatures. This review first focuses on the significance of defects/functionalization, discussion of different allotropes, and overarching structure–property relationships of 2D main group elemental materials. Then, a complete review of emerging applications in electronics, sensing, spintronics, plasmonics, photodetectors, ultrafast lasers, batteries, supercapacitors, and thermoelectrics is presented by application type, including detailed descriptions of how the material properties may be tailored toward each specific application.

1. Introduction

Often regarded as a new area of research, the field of elemental 2D materials is in fact undergoing a reawakening. Research into elemental monolayers can be traced back to the 1930s to the pioneering work of Langmuir, who studied the formation of alkali metal atoms on metal films and laid down the foundations of the field of surface science.[1] In the ensuing years, surface scientists studied the formation and properties (chemical, electronic, and optical) of a large number of metal monolayers on a variety of metallic substrates.[2] While the study of elemental monolayers, and 2D materials, in general has largely been in the domain of surface science, the successful isolation and study of the fascinating electronic and thermal properties of monolayer graphene[3] have led to a resurgence of interest in layered 2D materials including transition metal oxides, chalcogenides, and MXenes.[4–7] This interest has been generated by the discovery of new and exciting physics such as nontrivial topology,[8–10] high-temperature ballistic transport,[11,12] valleytronics,[13] and other optoelectronic[14] properties that arise predominantly due to their 2D nature; these have recently been discussed in a number of excellent reviews.[6,14–16] As a result, atomically thin materials are being targeted for a number of potential next-generation technology relevant applications, such as spintronics, advanced nanoelectronics, nanosensing, and many more.

Among layered 2D materials, research interest in elemental materials has rejuvenated over the past few years, driven largely by the search for atomically thin materials beyond graphene that exhibit unique and exciting properties.[17] The successful experimental realization of nongraphene elemental 2D-analogs such as silicene and phosphorene was the beginning of an ever-expanding list of elements that have been predicted or synthesized in atomically thin form. To date, the existence of 15 elemental main group 2D materials has been experimentally

Dr. N. R. Glavin, Dr. R. Rao, Dr. V. Varshney, Dr. A. Roy
Materials and Manufacturing Directorate
Air Force Research Laboratory
Wright-Patterson AFB, OH 45433, USA
E-mail: nicholas.glavin.1@us.af.mil
Dr. R. Rao
UES Inc.
Beavercreek, OH 45431, USA
Dr. E. Bianco, Prof. E. Ringe
Department of Chemistry
Rice University
Houston, TX 77005, USA
Dr. E. Bianco, Dr. A. Apte, Prof. P. M. Ajayan
Materials Science and Nano Engineering
Rice University
Houston, TX 77005, USA
E-mail: pma2@rice.edu
Prof. E. Ringe
Department of Materials Science and Metallurgy
University of Cambridge
Cambridge CB3 0FS, UK
Prof. E. Ringe
Department of Earth Sciences
University of Cambridge
Cambridge CB2 3EQ, UK
The ORCID identification number(s) for the author(s) of this article can be found under https://doi.org/10.1002/adma.201904302.

DOI: 10.1002/adma.201904302

verified or theoretically predicted, with a variety of intriguing and useful applications, as shown in **Figure 1**a. Figure 1b depicts the timeline of successful experimental and, if they have yet to be experimentally isolated, theoretical predictions the 2D elemental materials to date in the postgraphene era to the best of our knowledge.[18–31] While many of these were hypothesized to exist prior to the "reawakening" of 2D materials triggered by the initial work on graphene, recent work in the 2D materials field has shaped the future of these atomically thin materials. Last, note that this review discussion focuses specifically on the main group elements and does not explicitly discuss 2D elemental transition metals, which were reviewed elsewhere recently.[5,32]

Motivated by recent advances in the exciting class of main group elemental materials, herein we review the application literature to date, connect the crystal structure of various elemental 2D materials to their measured/predicted properties, and identify their strengths and weaknesses for applications including electronics, spintronics, optoelectronics, energy conversion, and more.

2. Crystal Allotropes of Elemental 2D Materials

The material properties (electronic, optical, and thermal, etc.) of elemental 2D materials are not simply dictated by their chemical makeup but also are strongly correlated to their allotropes, i.e., how atoms are arranged in the lattice. Similar to their 3D analogs, all studied elemental 2D materials have either been shown or been theoretically proposed to possess allotropes of differing crystal lattices. In this context, **Figure 2** showcases various examples of crystal lattices spanning the range of experimentally or theoretically explored 2D materials reported here.

While all elements in Group IV share electronic features similar to its lightest element, C, the favorable hybridization state for Si, Ge, and Sn is somewhere between sp^2 and sp^3. This leads to buckled crystal lattice structures rather than planar as observed in graphene,[40,41] although a planar polymorph of 2D Sn has also been experimentally synthesized on silver substrates.[42] In a recent study, Matusalem et al. suggested the MoS_2-like symmetry to be most stable for stanene, while large honeycomb dumb-bell (LHD) geometry (Figure 2) was reported to be more stable for silicene and germanene.[36] For "non-graphene" 2D carbon, Figure 2 shows the two most theoretically studied polymorphs, namely phagraphene (consisting of pentagons, hexagons, and heptagons) and penta-graphene (consisting entirely of pentagons), among several others, although neither has been experimentally realized to date. While theoretical studies predict that these phases are potential stable (although relatively less so than graphene), external stimuli or intrinsic defects may substantially reduce their stability. For example, Rahaman et al. suggested that applying uniaxial loading transforms penta-graphene to a more energetically stable metallic isomer, biphynylene,[43] while Shahrokhi et al. predicted that penta-graphene becomes much less stable under strain.[44]

Among group III elements, especially for 2D aluminum (aluminene) and 2D boron (borophene), a number of allotropes have been theoretically predicted with somewhat complex multiatomic unit cells. This complexity may possibly be related to lower number of valence electrons (3) in group III elements, resulting in their unique electronic band structures.[45] Recently, 2D gallium (gallenene) also has shown to possess two stable polymorphs, one with a buckled and the other with a planar 2D configuration (Figure 2).

Figure 2 also shows different 2D allotropes for group V elements, which have been studied in the recent literature. Among them, buckled (α-form) and puckered (β-form) lattices have been noted as most stable for all group V elements,

Nicholas R. Glavin received his Ph.D. in mechanical engineering from the University of Purdue in 2016. Upon completion, he joined the Functional Materials Division at the Air Force Research Laboratory, where his group is currently focused on the synthesis, processing, and characterization of 2D and III–V materials for flexible electronics and sensors.

Rahul Rao received his Ph.D. in physics from Clemson University in 2007. He was a National Research Council postdoctoral fellow at the Air Force Research Laboratory, and then joined the Honda Research Institute as a senior scientist. In 2015, he returned to AFRL and has since focused his research efforts on developing in situ methods for the synthesis and processing of nanomaterials including carbon nanotubes, graphene, and other 2D materials.

Pulickel M. Ajayan received his Ph.D. in materials science and engineering from Northwestern University in 1989. Shortly after, he joined the materials science and engineering faculty at Rensselaer Polytechnic Institute as an assistant professor. Currently, he is the founding chair of the Materials Science and Nanoengineering Department and the Benjamin M. and Mary Greenwood Anderson Professor in Engineering at Rice University. His research interests are focused on the functional nanostructured materials for a variety of applications.

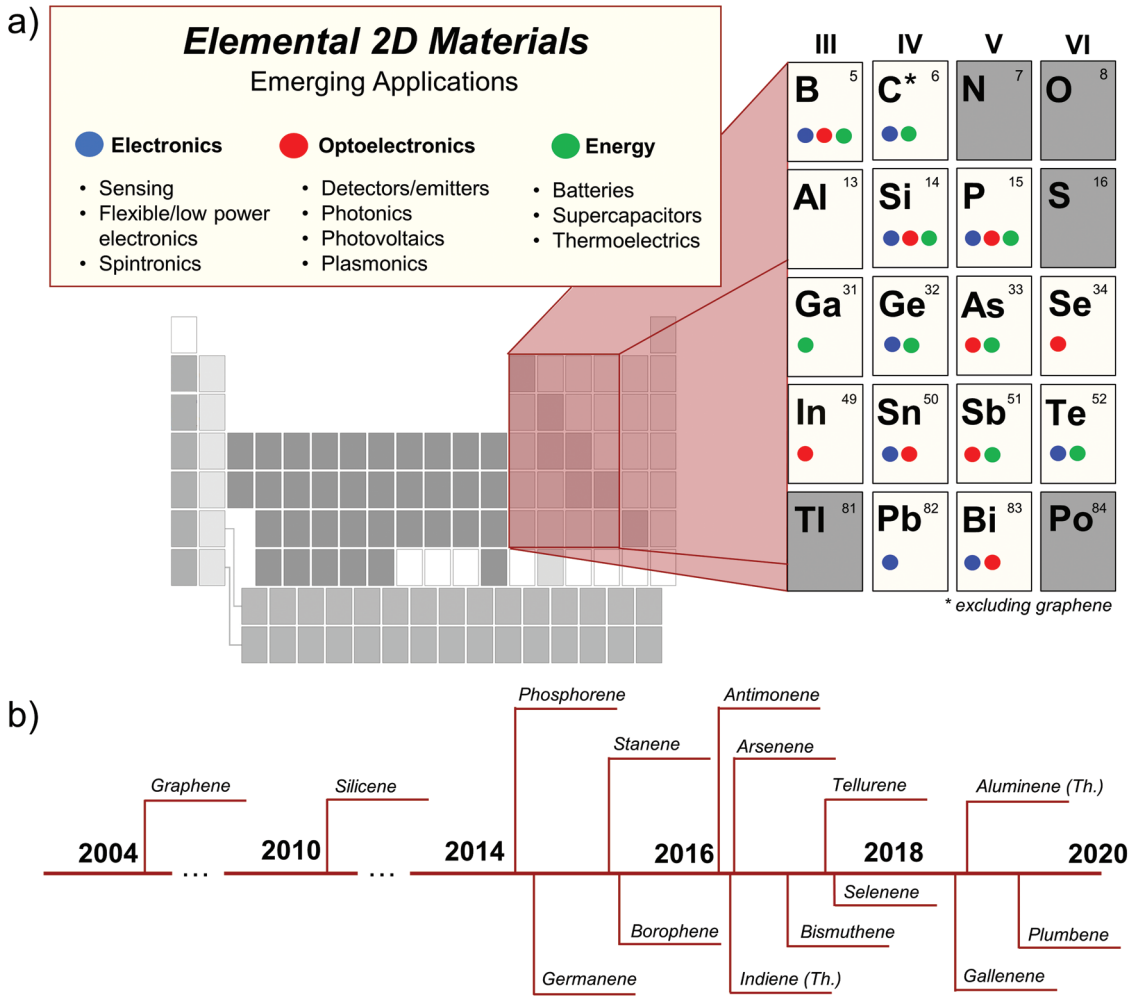

Figure 1. a) Overview of 2D analogues of main-group elements, explored either via experimental or theoretical routes in literature. Each colored circle within the elemental box is indicative of different application areas explored in the literature. The dark, shaded elements have not been explored so far. It should be noted that the well-known allotrope of carbon, i.e., graphene, is excluded from consideration in this study. b) A timeline of experimental realization of several recent elemental 2D materials after the isolation of graphene where "Th." means theoretical. Data taken from refs. [18–20,22–31,33].

although for arsenene, a γ-form and a δ-form has also been proposed. The puckered structure of the group V elemental 2D materials arsenene, bismuthene, and antimonene are predicted to exhibit ferroelectric (and even antiferroelectric in bismuthene) properties with Curie temperature above room temperature, an advancement that, if experimentally realized, would revolutionize the application space of elemental 2D materials.[46] Of the group V elements, air stability remains a common issue. Phosphorene, the puckered or "black" phase, for instance, has been extensively investigated but remains highly susceptible to oxidation in air, making encapsulation schemes necessary.[47–49] Meanwhile, antimonene crystals with buckled structure have been shown to be stable in air and chemically robust.[50] In addition, crystal forms of antimonene have been predicted to have different degrees of anisotropy in mechanical properties.[51] The largest of the group V elements, bismuthene, has been theoretically predicted and experimentally determined to exist in the buckled (Bi(111)) as well as the puckered (Bi(110)) phase, with a relatively high degree of air stability.[26,52,53]

A number of 2D allotropic forms have been recently proposed for the group VI elements, Te and Se, including their bulk-like helical configuration of covalently bonded atoms spiraling along the *c*-axis.[54] In contrast, Zhu et al. and Xian et al. both published separate computational studies of 2D Te allotropes[27,39] predicting similar potential 2D structures with compelling properties and varying stability. Xian et al. suggested that the most stable low-dimensional allotrope is an isolated 1D helical chain (the building block of the bulk structure) for both Se and Te; however, some true 2D structures were also predicted to be attainable such as "rectangular tellurene" and "square tellurene" (see Figure 2) with their respective cohesive energies of 0.06 eV per atom and 0.13 eV per atom higher than 1D chains. Synthesized ultrathin Te films by both PLD and PVD techniques exhibited the α-type stacking along with the existence of various other polymorphs.[55] Similar to other elemental 2D materials, "square" selenene and tellurene were predicted to be more stable in their nonplanar (buckled) configuration. In addition, these metastable phases were proposed to be energetically favorable enough to possibly be stabilized by proper

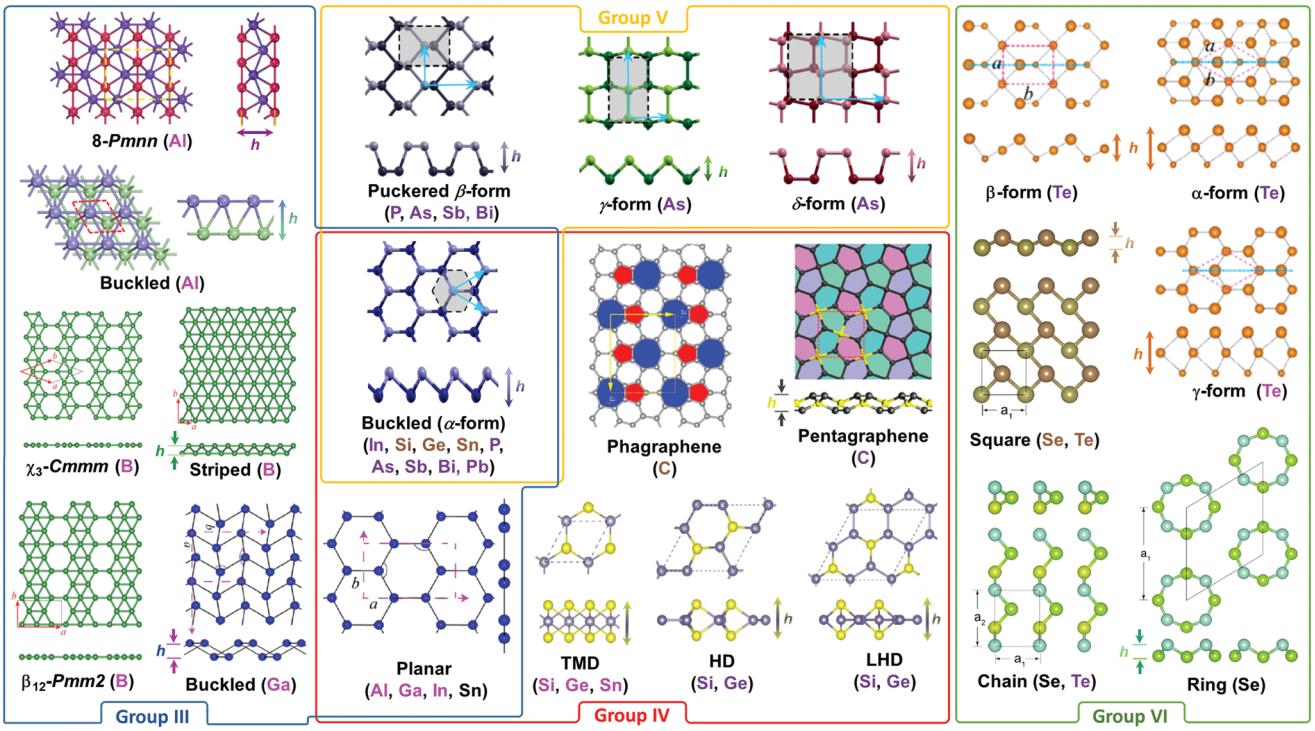

Figure 2. Allotropes of various main group elemental 2D materials. Different crystal lattices are shown along with various elemental 2D materials, which have been either experimentally realized or theoretically proposed for each crystal lattice type. The color of each element in parentheses characterizes the electronic behavior of a particular lattice type pertaining to that element. Color scheme: metal (pink); semimetal (brown) semi-conductor (purple); unknown (black). Image for "α-/β-/γ-form" (Group VI): Reproduced with permission.[27] Copyright 2017, American Physical Society. Images for "Buckled-Ga" (Group III) and "Planar" (Group IV): Reproduced with permission.[29] Copyright 2018, The Authors, published by American Association for the Advancement of Science (AAAS). Reprinted/adapted from ref. [29]. © The Authors, some rights reserved; exclusive licensee American Association for the Advancement of Science. Distributed under a Creative Commons Attribution NonCommercial License 4.0 (CC BY-NC) http://creativecommons.org/licenses/by-nc/4.0/. Image for "χ3-Cmmm/β12-Pmm2/Striped" (Group III): Reproduced with permission.[34] Copyright 2016, Informa UK Limited, trading as Taylor & Francis Group. Image for "8-Pmnn & Buckled-Al" (Group III): Reproduced with permission.[35] Copyright 2019, American Physical Society. Image for "TMD/HD/LHD form" (Group IV): Reproduced with permission.[36] Copyright 2015, American Physical Society. Image for "Penta-graphene" (Group IV): Reproduced with permission.[37] Copyright 2015, National Academy of Sciences. Image for "Phagraphene" (Group IV): Reproduced with permission.[38] Copyright 2015, American Chemical Society. Image for "Square/Chain/Ring": (Group IV): Reproduced with permission.[39] Copyright IOP Publishing. Image for "α-(Buckled))/β-(Puckered)/γ-/δ-form" (Group V): Reproduced with permission.[111] Copyright 2016, American Physical Society.

epitaxially-matched substrates, such as Au. Zhu et al. predicted three possible 2D reconstructions of the Te lattice at "magic thicknesses" of $N = 3$, 6, 9, 12, and 15 atoms: a stable hexagonal α-type, metastable rectangular β-type, and a metastable hexagonal γ-type reconstruction (Figure 2). These "magic" thicknesses were attributed to the multivalent nature of Te, in which the center atoms exhibit a metallic, σ-bonding character while the outer two atoms bond to the central atom with a more metal–ligand type nature. Recently, predicted allotropes of selenene suggest that C–Se, a tiled 1D chain geometry, may possess ferroelectric properties with a spontaneous in-plane ferroelectric polarization of about 2.68×10^{-10} C m^{-1} per layer.[56]

3. Synthesis of Elemental 2D Materials

In this section, we provide a brief overview of different synthesis routes that have led to elemental 2D analogs of different group III–VI elements, starting with graphene and group IV, then moving to group III, V, and VI in succession. An atlas of successful experimental realization of these materials is shown in **Figure 3**. We start our discussion with one of the first and most discussed "non-graphene" 2D material, silicene, a main group IV 2D analog of silicon. Initially, silicene was grown as nanoribbons on metallic substrates, and following this both silicene as well as its next group IV neighbor, germanene have been grown by molecular beam epitaxy (MBE) on a variety of substrates.[20,57–63] Synthesis of silicene has proven to be rather limited by this technique, with only a few demonstrations on metal surfaces,[61] graphite,[64] and silicon.[57] Different polymorphs of germanene such as flat germanene exhibiting differing surface reconstructions (on Au (111) and Al (111) surfaces) as well as distorted germanene (on Pt (111)) has been grown via MBE on metal substrates (see Figure 2 for various polymorphs).[20,58–60] In 2016, Zhang et al. demonstrated the first growth of buckled germanene on nonmetallic substrates (MoS_2) affording experimental evidence of the predicted Dirac cone via scanning tunneling spectroscopy (STS).[65] Kaloni and Schwingenschlögl predicted that H-passivation of GaAs (0001) surface and subsequent growth could lead to exfoliable germanene.[66]

Apart from graphene, many different 2D analogues of elemental carbon[74–78] have been proposed to date theoretically,

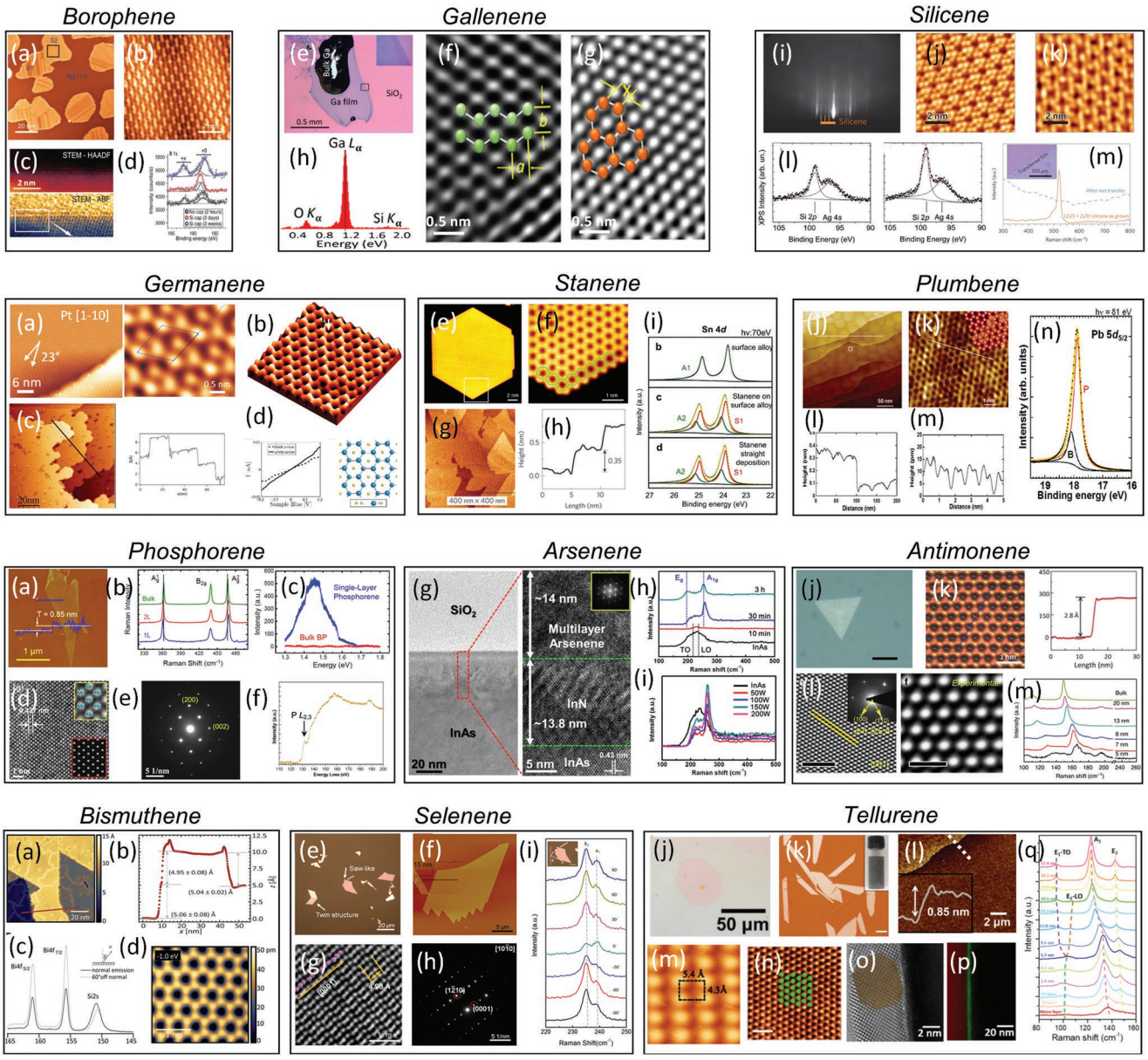

Figure 3. An atlas of experimentally realized elemental 2D materials. **Row 1**: Borophene: a) STM image of borophene sheets annealed at 650K; b) Atomic resolution STM image; c) Cross-section high-angle dark-field scanning transmission electron microscopy (HAADF-STEM) image of borophene sheet; d) Angle-resolved X-ray photoelectron spectrum (XPS) spectra of Si-capped borophene. Gallenene: e) Optical image of gallenene exfoliated from bulk Ga droplet on SiO_2/Si substrate; f,g) High-resolution transmission electron microscopy (HRTEM) images of a_{100} and b_{010} gallenene; h) Energy-dispersive X-ray spectroscopy (EDS) spectrum showing presence of Ga. Silicene: i) Reflection high-energy electron diffraction (RHEED (pattern of silicene on Ag (111); j,k) STM image of silicene with 4×4 and $\sqrt{13} \times \sqrt{13}$ reconstructions. l) XPS spectra of silicene on Ag (111); m) Raman spectra of as-exfoliated $2\sqrt{3} \times 2\sqrt{3}$ silicene. a,b) Reproduced with permission.[67] Copyright 2016, Springer Nature. c,d) Reproduced with permission.[23] Copyright 2015, AAAS. e–h) Reproduced with permission.[29] Copyright 2018, The Authors, published by American Association for the Advancement of Science (AAAS). Reprinted/adapted from ref. [29]. © The Authors, some rights reserved; exclusive licensee American Association for the Advancement of Science. Distributed under a Creative Commons Attribution NonCommercial License 4.0 (CC BY-NC) http://creativecommons.org/licenses/by-nc/4.0/. i,j,k,m) Reproduced with permission.[68] Copyright 2015, Springer Nature. l) Reproduced with permission.[57] Copyright 2012, Wiley-VCH. **Row 2**: Germanene: a) STM image of germanene grown on Pt (111). b) STM image of honeycomb lattice of germanene on Ge_2Pt. c) STM image of germanene on Au (111) with 0.3 nm steps. d) IV curves from vertex and center of honeycomb lattice in (b). Stanene: e–j) STM images of stanene flakes on Cu (111) and Bi_2Te_3. k) XPS of stanene on Ag (111) surface with underlying Ag_2Sn alloy. l) Raman spectra of pure and oxidized stanene flakes produced via liquid exfoliation. Plumbene: j–m) STM images of plumbene on Pd (111) resulting from the formation of a bubble-like surface of $Pd_{1-x}Pb_x$ surface alloy. The plumbene layer shows expected honeycomb structure with lattice constant of 0.49 nm. n) XPS core-level spectrum of Pb 5d showing two fitted components arising out of the $Pd_{1-x}Pb_x$ surface alloy and plumbene layer. a) Reproduced with permission.[60] Copyright 2014, Wiley-VCH. b,d) Reproduced with permission.[58] Copyright 2014, Institute of Physics. c) Reproduced under the terms of the CC-BY Creative Commons Attribution 4.0 International License (http://creativecommons.org/licenses/by/4.0/).[69] Copyright 2018, Springer Nature. e,f) Reproduced with permission.[70] Copyright 2018, Springer Nature. g,h) Reproduced with permission.[22] Copyright 2015, Springer Nature. i) Reproduced under the terms of the CC-BY

although none with any experimental success to date. Among them, penta-graphene has been extensively explored theoretically. However, it was predicted that penta-graphene may not be experimentally achievable as it could be difficult to isolate from the plethora of alternate carbon isomers with similar energies, which could all rapidly restructure to graphene.[79] Furthermore, viable strategies to stabilize penta-graphene have not yet been identified. The group IV element stanene has received considerable theoretical and experimental attention in the literature due to the suggestion of a topological insulator at room temperature as well as spin filtering and giant magnetoresistance, courtesy of the large spin–orbit coupling from the heavy tin atoms.[80,81] Zhu et al. reported the growth of 0.35 nm thick buckled diatomic stanene on bismuth telluride via molecular beam epitaxy (MBE) and the existence of a bandgap within metallic states via scanning tunneling microscopy (STM).[22] This was followed by the growth of ultraflat layers stabilized on the metallic surfaces Cu (111) and Ag (111).[42,70] In the former study, the presence of Cu resulted in an inversion of the s & p bands, opening up a topological bandgap of 0.3 eV whereas in the latter, the buckling was eliminated due to presence of an Ag_2Sn alloy. Saxena et al. have reported the formation of ultrathin stanene nanosheets in hexane solution by laser ablation of bulk tin crystals.[82] The 0.33 nm thick sheets displayed strong optical absorption at 6.23 eV and good resistance to oxidation.

Among group III elements, only 2D analogues of boron (borophene) and gallium (gallenene) have been experimentally realized to date. Mannix et al. demonstrated the growth of buckled, ultrathin borophene sheets with vapor deposition on Ag (111) in ultrahigh vacuum at 550 °C with anisotropic metallic properties.[23] The initial deposition of borophene proved that the 2D material is naturally unstable, but efforts to encapsulate the films showed a successful delay of oxidation for days.[23] This was extended by Feng et al. where the as-grown β_{12} borophene sheets on Ag (111) with rectangular unit cell showed a structural phase transition at 650K to the χ^3-phase with in-plane zig-zag atomic arrangement.[67] Among other group III elements, Kochat et al. demonstrated exfoliation techniques to isolate atomically tin gallium, or gallenene, along the *a* and *b* crystallographic directions from melting droplet of bulk crystal near room temperature (T_m of Ga = 30 °C).[29] The exfoliated sheets displayed metallic conductivity and compatibility with a variety of substrates along with inducing a 2H-1T structural phase transition when coupled as a heterostructure with monolayer MoS_2. Kamal et al. theoretically studied the stability of aluminene and observed that the honeycomb lattice similar to that of graphene was most stable. This aluminene is predicted to behave like graphene with hole-doping, i.e., metallic along with potential superconductivity.[83]

In group V elemental 2D analogues, phosphorene is reported to be rather dissimilar to the remaining group V materials due to its lighter atomic mass. Liquid shear exfoliation of bulk black phosphorus has proven successful in isolating multilayer black phosphorous in solvents such as n-methyl pyrrolidone, dimethyl sulfoxide, and dimethyl formamide.[72,84] Phosphorene degrades in air via dissociative chemisorption of O_2.[85] Capping phosphorene with a dielectric (Al_2O_3) or fluoropolymer improves the stability of devices and transistors with indefinite air stability.[47] Following a computational work on the existence of blue phosphorus by Zhu and Tománek,[86] Zhang and co-workers[87] successfully synthesized single-layer blue phosphorus via MBE on Au (111) by using black phosphorus as a precursor. Taking one row down the group, multilayer arsenene nanoribbons have been synthesized on InAs substrates by exposure to N_2 plasma.[33] Also from Group V, few-layer (4 nm thick) antimonene has been grown on mica substrates by chemical vapor transport (CVT).[73] Fortin-Deschênes et al. described the growth of monolayer β-Sb on Ge (111) substrates[88] while Xu et al. successfully grew monolayer β-Sb on $PdTe_2$ by MBE.[50] Multilayer antimonene nanoribbons were grown on InSb substrates by exposure to N_2 plasma by Tsai et al.[89] Unlike other group III and V 2D materials, antimonene is likely to possess much better air stability, as Ji et al.[73] reported that few layer antimonene grown by CVT on mica substrates were air-stable up to 30 d. Xu et al. found that monolayer Sb on $PdTe_2$ substrates was chemically inert after annealing the substrates after MBE growth up to 380 K, observing that X-ray photoelectron spectroscopy (XPS) peaks (indicative of oxidation states) did not change over time.[50] Last, bismuthene, first synthesized in the 1970s, experienced a reawakening recently when it was successfully grown by MBE on SiC (0001) substrates.[26,90]

3.0 Attribution 3.0 Unported License (https://creativecommons.org/licenses/by/3.0/).[42] Copyright 2018, IOP Publishing Ltd. j–n) Reproduced with permission.[30] Copyright 2019, Wiley-VCH. **Row 3**: Phosphorene: a) Atomic force microscopy (AFM) image, Raman spectra, and photoluminescence of exfoliated phosphorene. d) HRTEM image, e) selected area electron diffraction (SAED), and f) core-loss electron energy loss spectrum of shear-exfoliated phosphorene. Arsenene: g) HRTEM image of few-layer arsenene grown on top of InAs substrate. h,i) Raman spectra of InAs substrate after N_2 plasma treatment and annealing at 450 °C showing presence of arsenene. Antimonene: j) Optical image, k) STM image, and l,m) HRTEM image showing atomically resolved antimonene lattice. m) Raman spectra of antimonene as function of thickness. a–c) Reproduced with permission.[71] Copyright 2014, American Chemical Society. d–f) Reproduced with permission.[72] Copyright 2016, Institute of Physics. g–i) Reproduced with permission.[33] Copyright 2016, American Chemical Society. j,l,m) Reproduced under the terms of the CC-BY Creative Commons Attribution 4.0 International License (http://creativecommons.org/licenses/by/4.0/).[73] Copyright 2016, The Authors, published by Springer Nature. k) Reproduced with permission.[50] Copyright 2016, Wiley-VCH. **Row 4**: Bismuthene: a,b) STM image and line profile of bismuthene on SiC (0001). c) Occupied state STM image of Bi honeycomb lattice. d) XPS spectrum of bismuthene on SiC (0001). Selenene: e,f) Optical and AFM images of selenene flakes. g,h) HAADF-STEM image and SAED pattern. i) Raman spectra of selenene showing polarization dependence. Tellurene: j,k) Optical images of PVD-grown and liquid-exfoliated tellurene. l) AFM image of PVD tellurene on SiO_2/Si substrate showing sub-nanometer thickness. m) STM image of tellurene on HOPG showing rectangular unit cell of beta polytype. n) HAADF-STEM image of PVD tellurene showing alpha polytype. o,p) Cross-sectional HRTEM image and EDS mapping of PLD tellurene on MgO (220) substrate. q) Raman spectra of liquid-exfoliated tellurene with thickness dependence. a–d) Reproduced with permission.[26] Copyright 2017, AAAS. e–i) Reproduced with permission.[28] Copyright 2017, American Chemical Society. j,l,n–p) Reproduced with permission.[55] Copyright 2018, Institute of Physics. k,q) Reproduced with permission.[91] Copyright 2018, Springer Nature. m) Reproduced with permission.[27] Copyright 2017, American Physical Society.

For group VI elements, synthesis efforts have focused on 2D analogs of selenium (Se) and tellurium (Te).[27,28,55,91,92] Tellurene thin films with a thickness, t, ≈10 nm were grown by high-vacuum thermal evaporation dating back in the 1970s[93] while selenium monolayers were electrochemically deposited on Au (111) in 1997.[94] However, prior to the discovery of exciting 2D physics, the stability and properties of 2D and ultrathin (t < 10 nm) allotropes were not deeply explored nor their structures heavily pursued. Recently, Zhu et al. and Chen et al. have demonstrated the growth of β-type tellurene on highly oriented pyrolytic graphite (HOPG) substrates while Huang et al. demonstrated monolayers of tellurene with the <0001> helical chains oriented in the substrate plane on graphene/6H-SiC(0001) substrates grown by MBE.[27,91,92] Wang et al. showed solution-phase growth of free-standing micron scale tellurene single crystals tens of nm thick, which could undergo a postthinning process to near monolayer (≈0.5 nm) thickness.[91] Qin et al. demonstrated vapor phase deposition of selenene flakes, t = 5–15 nm and lateral dimensions ≈10 µm, in a tube furnace at ≈200 °C under flowing Ar.[28] These flakes exhibited lateral growth along[1–208] direction, which was attributed to the large mean free path of the gaseous Se species at high temperature.[28,91,92,95,96]

4. Unique Properties of Elemental 2D Materials

The lattice structures of elemental 2D materials along with differences in valence electrons and their relative energies give rise to a plethora of interesting properties. Below, we discuss the current state-of-the-art in terms of electronic, optical, and magnetic properties exhibited by 2D structures and how different external stimuli, such as strain, doping, passivation, functionalization, and stacking arrangements can be employed to modulate and/or transform such properties.

Bandgap: As we move across the periodic table from group III to group VI, the general trend of monolayer 2D materials observed is a transition from metallic to semimetal to semiconducting behavior. These specific details for all reported 2D allotropes are depicted in **Figure 4** for materials at the monolayer thickness and additional details are shown in Table S1, Supporting Information. For example, borophene, aluminene, and gallenene (all group III) are all either measured or predicted to be metallic in nature.[23,97] Similarly, all Group IV 2D materials with buckled lattice structure also possess Dirac cone semimetal band structures similar to graphene, with the possibilities of bandgap modulation through various external stimuli (discussed later).[98–100] Interestingly, "non-graphene" carbon allotropes have been predicted to possess varied electronic band-structures ranging from metallic (α-phographene,[75] Psi-graphene,[77] phagraphene,[101] and others[78]) to wide-bandgap semiconductors (twin-graphene (≈1 eV)[76] and penta-graphene (≈3.25 eV)).[74] Such differences can be attributed to different degrees of sp^2/sp^3 hybridization, as well as varying degree of resonance in predicted 2D crystal lattices of elemental carbon.

In group V, monolayer black and blue phosphorous, respectively, exhibit an experimental bandgap of 1.88 and 1.10 eV.[87,115] With increasing layers, this bandgap lowers significantly as is the case with bulk black phosphorus has a bandgap of 0.3 eV.[115] Arsenene has been predicted to possess an indirect, quasi-particle bandgap of ≈2.5 eV[116] while antimonene is predicted to have an indirect bandgap around 2.3 eV.[21] Bismuthene, their heavier counterpart, has been predicted to achieve room-temperature topological

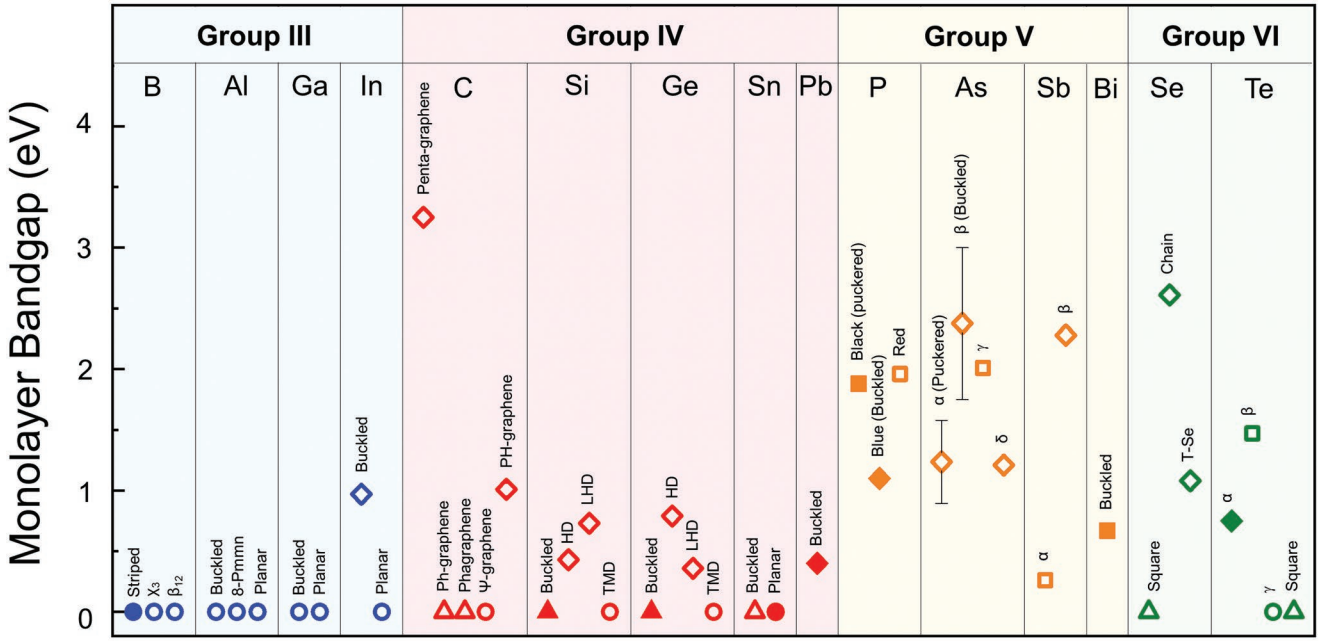

Figure 4. Electronic bandgaps of monolayer elemental 2D materials and their structural variants. The corresponding symbols depict the following: Closed symbol—monolayer material has been experimentally isolated; open symbol—monolayer material has yet to be experimentally isolated, ● metal, ▲ semimetal, ♦ indirect bandgap, ■ direct bandgap. Error bars are associated with differing predicted values. Bandgap values taken from refs. [21,27,29,34–36,38–40,74,77,87,91,102–115].

insulating behavior (see below) with a predicted spin–orbit monolayer bandgap of ≈0.3 eV[26,52] and measured bandgap of 0.67 eV,[26] which disappears in multilayer bismuthene as it becomes metallic. In group VI elements, α- and β-tellurene (see Figure 2) has been predicted to have a "nearly direct" and direct bandgap of 0.75 and 1.47 eV, respectively. Experimentally, monolayers of tellurene with helical chains (<0001> direction) aligned along the substrate plane have been shown to have a bandgap as large as ≈1 eV (vs 0.34 eV in bulk) by STS, which monotonically decreases toward the bulk value with increasing Te thickness.[92] Such a behavior opens the possibility for thickness-dependent optical bandgap tuning from IR up to near-IR region.

Spin–Orbit Coupling: Group IV 2D analogues with semimetallic band structure have been predicted to exhibit some degree of spin–orbit coupling (SOC) leading to opening of a small bandgap around Dirac cone, which increases with their atomic number, i.e., C < Si < G < Sn, giving rise to possibility for realization of the quantum spin Hall effect (QSHE).[117,118] Heavier elemental 2D materials within the group IV, V, and VI elements (plumbene, bismuthene, selenene, and tellurene) have also been shown to exhibit a large spin–orbit coupling.[26,30,52,80] In group IV elements, silicene is predicted to have a spin–orbit gap of 1.55 meV, while germanene is predicted to have one of 23.9 meV in freestanding form. Furthermore, this gap is expected to be nearly as large in freestanding bi- and trilayer germanene.[119] While silicene and germanene also possess nonzero Z_2 invariants and therefore the possibility for the QSHE, their small spin–orbit splitting makes it only possible at low temperature.[120] Stanene, however, has been predicted to possess an appreciable spin–orbit gap of around 70 meV.[40,41,121,122]

In addition to their intrinsic spin–orbit coupling, substrates and stacking arrangements can modify the energy of the spin–orbit gap. For example, germanene grown on GaAs (0001) is expected to have a much larger spin–orbit gap of 175 meV, shifted 268 meV above the Fermi level.[66] Similarly, the spin–orbit gap of silicene is predicted to be up to 57 meV due to breaking of sublattice symmetry.[123] The energy of the spin–orbit gap of germanene on MoS_2 is predicted to also depend on the crystallographic orientation of the substrate.[119] As 2D materials interact very strongly with their underlying substrate, which certainly affects the degree of spin–orbit coupling, it has led to the development of passivation strategies to isolate freestanding forms[66] as well as functionalized derivatives of elemental 2D materials. For example, Xiong et al. modeled electronic properties of stanene nanoribbons (NRs) and found that both bare and edge-hydrogenated NRs were semiconducting in nature, although including spin–orbit coupling had different response to NRs.[124] While SOC opened the bandgap of zig-zag NRs, it reduced the bandgap for arm-chair NRs. Wang et al. predicted that QSHE can be induced in stanene under strain, however, they noted that in addition to tensile/compressive strain, the lattice matching of the substrate is extremely important as well.[99]

In the theoretically predicted buckled square lattice, square selenene and tellurene (group VI) exhibit anisotropic Dirac cone dispersions near the Fermi level at P_1 along the $\Gamma\mu_1$ direction, in which, upon considering SOC (in both cases), leads to opening a bandgap of ≈0.1 eV, similar to stanene.[80] These factors are the recipe for a 2D topological insulator (TI). TI band topology, which is also characterized by a nonzero Z_2 invariant, is calculated to be one in both square systems. In addition, the ≈0.1 eV gap in square selenene and tellurene polymorphs is large enough to realize the QSHE at room temperature, a discovery that could revolutionize the field of exotic electronics and spintronics.

Magnetic Properties: Several magnetic characteristics have been theoretically predicted in elemental 2D materials, primarily from group IV elements. For example, Wang et al. predicted that semi-hydrogenated (passivated at one edge) silicene and germanene to be ferromagnetic semiconductors with Curie temperatures of T_c = 122 K and 145 K, respectively.[125] Zig-zag germanene NRs were predicted to be ground state antiferromagnetic, while armchair NRs nonmagnetic in nature. Further, semiconducting zig-zag germanene NRs were predicted to become ferromagnetic semiconductors (or semimetals) with single-atom N or B edge doping.[126]

Xiong et al. modeled the magnetic properties of stanene NRs and predicted the zigzag NRs to be ground state ferromagnetic with opposite spin order between the two edges.[124] Xing et al. modeled the adsorption of a number of transition metals onto the surface of stanene and suggested that while most metals survived the magnetic moment on adsorption, Ni, Cu, and Zn made stanene nonmagnetic. In particular, Fe-absorbed stanene was found to be a bipolar magnetic gapless semiconductor with up-spin electrons and down-spin hole carriers. This phenomenon supports the coexistence of the charge and pure spin current, which may have great potential for electrically controllable spintronic devices.[127] For stanene NRs, Fu et al. obtained four types of edge magnetic configurations out-of-plane ferromagnetic (OP-FM), out-of-plane anti-ferromagnetic (OP-AFM), in-plane ferromagnetic (IP-FM), and in-plane antiferromagnetic (IP-AFM).[117] All four magnetic states were predicted to be ≈7–8 meV per edge atom lower energy than the nonmagnetic states, suggesting spontaneous magnetism. On applying transverse electric field, half-metallic states could be induced in nanoribbons, which has promising prospects in magnetic control and spintronics.[117] In a recent study, interaction of various gases with stanene was investigated by Garg et al. where the author found that stanene gas systems show Rashba type spin-splitting, which is very promising for spintronics applications.[128]

He et al. numerically studied the magnetic behavior of pentagraphene nanoribbons and suggested that their spin moments can transform from ferromagnetic to antiferromagnetic under electric field and bending strain, which may have applications in flexible displays, wearable computation electronics, and digital memory devices.[129] In another carbon 2D allotrope study, Aierken theoretically studied penta-hexagraphene and predicted that it possesses intrinsic antiferromagnetism, which could be transformed to ferromagnetism by applied in-plane strain, also suggesting its potential in metal-free magnetic monolayer materials for spintronic devices.[130]

5. Modulation of Electronic Bandgap in 2D Materials

Bandgaps in nanoscale materials play a vital role in optoelectronic properties and dictate their potential future applications. Similar to modifying degree of spin–orbit coupling in

semimetals, a number of strategies have been undertaken via theoretical modeling in all instances unless otherwise stated, to modulate (or open) the bandgap of elemental 2D materials. This section specifically addresses the influence of strain, electric field, functionalization, doping, edge, and/or surface passivation as a means to modulate this bandgap toward enabling new and exciting applications.

Strain: In semimetallic germanene, tensile strain of up to 16% was predicted to shift the Dirac point above the Fermi level, inducing p-type behavior due to decreased sp hybridization and increased Ge–Ge bond length.[131,132] Broek et al. suggested that applying lateral strain on stanene under out-of-plane electric field can open up the bandgap up to 0.21 eV,[41] while Modarresi and co-workers suggested that the SOC bandgap of ≈0.07 eV in stanene closes under applied strain.[122] Fu et al. studied stanene and predicted a metal–insulator transition under critical biaxial strain.[117] For penta-graphene NRs, the bandgap was shown to decrease with tensile and bending strain.[129,133] Shahrokhi predicted that biaxial tensile strain increases the bandgap of penta-graphene while compressive strain reduces the bandgap.[44] Among other carbon allotropes, psi-graphene was predicted to be metallic even under in-plane strain,[77] while bandgap could be tuned for semiconducting twin-graphene (≈1 eV) via applying strain.[76] For group V elements, monolayer antimonene was predicted to have a 2.3 eV indirect bandgap that undergoes an indirect-to-direct transition under strain.[21]

Electric Field: It has been theoretically predicted that application of electronic gating (out-of-plane electric field) can manipulate the band structure in silicene and germanene,[105,134] unlike graphene, which are unaffected by external vertical electrical field. For monolayer silicene, a bandgap varies linearly with electric field strength and a total gap as high as 18 meV was predicted, which could be increased to 0.25 eV at electric field strengths of 1 V Å^{-1} when sandwiched between *h*-BN layers.[105] Fu et al. studied the electronic and topological properties of stanene and predicted a topological nontrivial–trivial transition under a critical vertical electric field.[117]

Inclusion of Heteroatoms: In addition to strain and electric field, different strategies of including heteroatoms such as doping, adsorption, and surface passivation has been predicted to modify electronic band structure of elemental 2D materials. For example, Berdiyorov et al. investigated substitutional doping of penta-graphene via Si, B, and N and predicted a bandgap reduction, although its magnitude depends on the types and location of the dopants.[135] On the other hand, the authors, in accordance with a study by Li et al. found that surface termination via F and H increases the bandgap and considerably changes the electronic charge distribution.[136] Luo et al. studied doping of B and N in phagraphene NRs and predicted that while B-doping removed/changed the bandgap depending on doping position, N or BN doping increased the bandgap.[137] Garg et al. patterned stanene with BN doping and predicted a bandgap opening of ≈0.22 eV, and a semiconducting behavior sustained under applied strain.[138]

Other routes, such as hydrogenation and transition metal adsorption, have also been studied for multiple elemental 2D materials. Wang et al. studied partially hydrogenated (on one side) silicene and germanene and predicted direct bandgaps of 1.74 eV and 1.32 eV, respectively.[125] Fan et al. studied α-phographene and suggested it to be metallic in nature, which could be converted to wide bandgap semiconductor via hydrogenation.[75] Wu et al. studied the surface termination of phagraphene and predicted better stability and bandgap modulation to either semiconductor or insulator.[101] Xing et al. modeled the adsorption of a number of transition metals on stanene toward changing electronic properties and predicted that V, Cr, Mn, and Cu turn stanene into a metal, Co into a semimetal, while Ni and Zn open a narrow bandgap.[127] Apart from heteroatom inclusion, surface functionalization has also been used to manipulate bandgap in silicene, germanene,[139,140] and borophene.[141]

Modifying Nanoribbon Width and Stacking Arrangements: Borrowing concepts well known in the graphene community, 2D elemental materials may exhibit bandgap opening via quantum confinement and edge effects from creating nanoribbons.[142] Kaneko et al. predicted to open a bandgap of up to ≈1.0 eV in germanene NRs with reducing their width from 20 to 3 atoms.[143] Rajbanshi et al. studied penta-graphene nanoribbons and also suggested that the bandgap increases with reducing nanoribbon width.[133] On the contrary, Fu et al. predicted that for stanene NRs, edge states have a dispersion width of ≈83 meV, regardless of ribbon width.[117] Yu et al. suggested that bandgap in penta-graphene could be modulated by up to a factor of 2–3 by manipulating number of layers, stacking arrangement as well as their misalignment.[144]

6. Electronics and Sensing

The unique and exceptional properties of elemental 2D materials are poised to enable future advancements in electronics and sensing for beyond silicon devices. Many of the elemental 2D materials exhibit advantageous properties including high electron and hole mobilities and on/off ratios, material flexibility, topological insulating behavior, and high sensitivities to adsorbed molecules that can revolutionize current state of the art systems. This section discusses applications relevant to electronic and sensing and provides a groundwork on enabling these technological developments.

Electrical properties of elemental 2D materials are traditionally evaluated through fabrication and measurement of the materials during field effect transistor (FET) operation. To date, FETs with active elemental 2D materials that have been synthesized include phosphorene, silicene, tellurene, and selenene, all exhibiting a wide range of mobilities and on/off ratios, as shown in **Figure 5**a. The first of these materials to demonstrate exceptional FET performance was few-layer phosphorene in 2014. This material simultaneously displayed a high on-current of 194 mA mm^{-1}, a high hole field-effect mobility of 286 cm^2 V^{-1} s^{-1}, and an on/off ratio of up to 10^4 at room temperature.[71] Shortly after, Li et al. measured an even higher hole mobility of up to 1000 cm^2 V^{-1} s^{-1} for 10 nm thick phosphorene FETs.[19] Building off these initial demonstrations, Gillgren et al. sandwiched the few-layer material between hBN layers and measured room temperature hole mobilities up to 4000 cm^2 V^{-1} s^{-1}, as shown in Figure 5b,c.[145] Monolayer phosphorene transistors are currently under development, predicted to exhibit ballistic quantum transport with a faster switching speed than some monolayer transition metal dichalcogenides.[146] One of the contributing factors

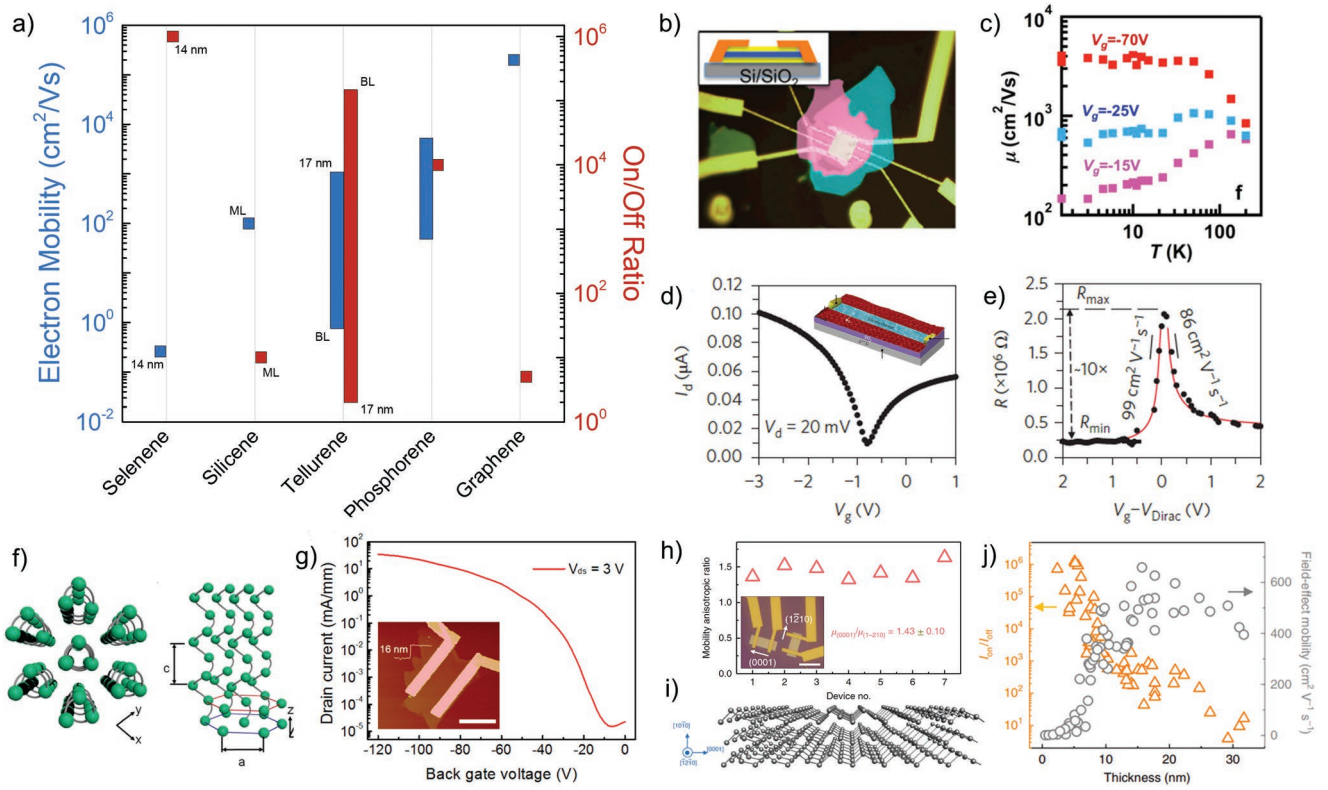

Figure 5. FET properties of elemental 2D materials. a) Compiled electron mobilities and on/off ratios of elemental 2D materials from refs. [39,68,71,91,145,148,149], where ML = monolayer, BL = bilayer, and the number legend corresponds to thickness. b) Optical image of h-BN/phosphorene heterostructure, and c) resulting electronic behavior at different temperatures. d) Device characteristics of monolayer silicone, and e) electron mobilities of the same devices. f) Crystallographic structure of 1D chains in 2D selenene with g) device characteristics of 16 nm 2D selinene. h) Anisotropic mobility behavior in 2D tellurene, i) atomic structure of tellurene, and j) thickness-dependent mobility and on/off ratio of 2D tellurene. b,c) Reproduced with permission.[145] Copyright 2014, IOP Publishing. d,e) Reproduced with permission.[68] Copyright 2015, Springer Nature. f,g) Reproduced with permission.[28] Copyright 2017, American Chemical Society. h–j) Reproduced with permission.[91] Copyright 2018, Springer Nature.

to the exceptional electronic performance in phosphorene and other monoelemental 2D materials is that unlike the 2D metal chalcogenide, the intrinsic point defects and grain boundaries in monoelemental materials are electrically inactive due to homoelemental bonding.[147]

Shortly after the first phosphorene transistor, monolayer silicene FETs operating in air were demonstrated by Tao et al. in 2015, and exhibited a mobility of 100 $cm^2\ V^{-1}\ s^{-1}$ (Figure 5d,e).[68] The mobility in this case was limited by acoustic phonon-limited transport and ambipolar Dirac charge transport similar to graphene.[68] This transistor demonstration represents the only FET measurement from a direct synthesized monolayer 2D elemental materials rather than exfoliated crystals to date, as is the case for all the monolayer FETs of phosphorene, tellurene and selenene. The silicene in the case was synthesized in mixed preferential orientations (4×4 and $\sqrt{13} \times \sqrt{13}$) through epitaxial growth on Ag (111) coated mica substrates and the devices were subsequently transferred to SiO_2. Additionally, in this study, the effects of encapsulation with Al_2O_3 was shown to prolong lifetime of the device and allow for transfer of the silicene films without damage. Further theoretical predictions indicate that the intrinsic properties of silicene may yield electron mobilities approaching 1200 $cm^2\ V^{-1}\ s^{-1}$, which would enable even more applications including RF electronics.[150] Electron–phonon coupling matrices predict that interaction of carriers with phonons is 25× less than in silicene and germanene as compared to graphene, which presumably leads to long momentum relaxation lengths and high carrier mobility.[151]

Following the demonstration of silicene FETs, transistors of both selenene and tellurene were fabricated on exfoliated crystals in early 2017. Devices with 16 nm thick selenene exhibited relatively low mobilities in comparison to other elemental 2D materials, (0.26 $cm^2\ V^{-1}\ s^{-1}$) and low on current (20 mA mm^{-1}), as depicted in Figure 5f,g, but a high on/off ratio $\approx 10^6$ at room temperature.[28] This ratio may be critical for logic-type devices where the on/off ratio is important to ensure low current leakage. Thickness-dependent electrical performance of tellurene crystals, in contrast, exhibited impressive and widely varying electronic performance and thickness-dependent optical properties not exhibited by typical layered 2D materials.[91] FETs with room-temperature mobility of 700 $cm^2\ V^{-1}\ s^{-1}$ (two times higher than initially measured phosphorene FETs) along the high-mobility (<0001>) direction (Figure 5h,i) have been shown in 16 nm thick solution-grown single crystals (Figure 5j). However, this performance is very sensitive to thickness, decreasing dramatically from 600 $cm^2\ V^{-1}\ s^{-1}$ in 15 nm crystals to 30 $cm^2\ V^{-1}\ s^{-1}$ in 5 nm crystals and continuing to decrease monotonically down to a monolayer. Tellurene crystals of thickness 7.5 nm exhibit p-type behavior with

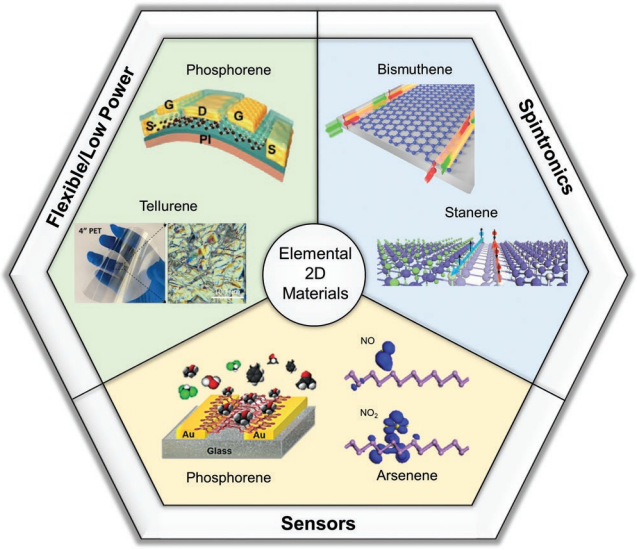

Figure 6. Advanced electronic applications of elemental 2D materials including flexile/low-power systems, spintronics, and sensors, and example elemental 2D materials of interest for specific applications. Image for "Phosphorene flexible/low power": Reproduced with permission.[155] Copyright 2016, American Chemical Society. Image for "Tellurene flexible low/power": Reproduced with permission.[91] Copyright 2018, Springer Nature. Image for "Bismuthene spintronics": Reproduced with permission.[26] Copyright 2017, AAAS. Image for "Stanene spintronics": Reproduced with permission.[80] Copyright 2013, American Physical Society. Image for "Phosphorene sensor": Reproduced with permission.[156] Copyright 2015, Wiley-VCH. Image for "Arsenene sensor": Reproduced with permission.[157] Copyright 2017, Elsevier.

on current of 300 mA mm^{-1} and on/off ratio of $\approx 10^5$.[91] From detailed Hall effect studies on tellurene thin films dating back to 1971, Dutton and Muller concluded from the relationship between mobility (μ) and temperature that ionized impurity scattering is the dominant scattering mechanism in tellurene thin films at room temperature, and from the linear relationship of μ and thickness, it was concluded that ionized impurities exist at the film surface in concentrations independent of film thickness.[152] As the thin film is reduced from relatively thick (3D), to ultrathin or 2D, geometries, surface events such as scattering become increasingly detrimental and may play a role in future monolayer tellurene electronic devices.

To date, three key areas of interests, depicted in **Figure 6**, have been explored leveraging these exceptional and diverse properties as future electronic and sensing platforms for 2D elemental materials: flexible/low power electronics, spintronics, and gas/chemical sensors. Other 2D materials have shown great promise in revolutionizing these fields including flexible low power electronics due to the inherent material flexibility, low turn-on voltage, and compatibility with polymer substrates.[153,154] Successful synthesis, processing, and integration schemes that are demonstrated for 2D transition metal chalcogenide materials and graphene will be the key to enabling these same concepts with elemental 2D materials, with potentially improved performance due to the advantageous properties and the ease of synthesizing monoelemental materials.

Flexible Electronics: The most challenging barriers to overcome for commercial development of elemental 2D flexible electronics are both in the preparation and synthesis of the materials on flexible substrates as well as an understanding of performance under repeated and dynamic strain. Hu et al. demonstrated a binder-free phosphorene ink by using isopropyl alcohol and 2-butanol as cosolvent that, coupled with the rapid drying of the solvents after inkjet printing, prevented the oxidation of the phosphorus, enabling stable inks.[158] They demonstrated printed phosphorene inks to operate as switches for ultrafast lasers, stable against intense irradiation, and as a visible to near-infrared photodetector with high responsivities. Further studies have even demonstrated phosphorene as a crucial material for flexible radio frequency electronics due to its high electron mobilities and good performance at high frequencies.[155] Tellurene was suspended in an Na_2TeO_3:PVP mixture and successfully 3D printed onto a flexible substrate, with future work necessary to optimize device performance on flexible substrates.[91] Incorporating growth and processing techniques that are commonplace in the flexible electronics community such as low temperature vacuum deposition or rapid thermal/photonic annealing may provide the mechanisms necessary to incorporate high quality materials on soft and compliant substrates, which cannot accommodate high growth temperatures.[159,160] Alternatively, the direct transfer of materials synthesized on conventional substrates (i.e., SiO_2/Si or sapphire) to flexible ones, through 2D van der Waals liftoff using materials such as *h*-BN, have been shown to enable high performing flexible electronic systems and may provide the key to flexible, low power electronics based on elemental 2D materials.[161–163]

Sensors: Gas and chemical sensors based on nanomaterials (especially 2D materials) exhibit a high degree of sensitivity from their large surface to volume ratio, high room temperature mobility, subthreshold swing in FET geometries, and chemical stability.[164,165] In particular, phosphorene gas sensors have demonstrated a high degree of sensitivity and selectivity in comparison to other nanomaterial sensors.[166] Mayorga-Martinez et al. fabricated a few-layer phosphorene device that proved to be selective to methanol and can detect as low as 28 ppm of methanol gas.[156] The phosphorene sensors in this two-terminal device operate on the premise that molecular adsorption can directly alter its electrochemical properties, in particular the electrical resistivity.[167] Phosphorene was also successful at detecting NO, NO_2, CO, CO_2, NH_3, and various other small molecules relying on this same premise of altering electrochemical and optical properties through molecular adsorption.[168–170] Other elemental 2D materials are predicted to exhibit advantageous sensing properties, but have yet to be fabricated and experimentally tested. Garg et al. modeled the potential effectiveness of B, N, and BN-doped stanene as a sensors for several gases, where doping provided both higher sensitivity and selectivity.[138] Arsenene has been predicted to be a promising candidate for sensing NO, NO_2, and SO_2, as the molecules interact strongly with the elemental 2D material and can create a measureable and detectable change in magnetic moment.[157,171] Semimetal 2D materials such as silicone and germanene provide for an interesting platform for sensing, as bandgaps can be opened and controlled specifically from molecular adsorption. For instance, DFT results predict that germanene is a candidate for gas sensing of NO and NH_3 due to moderate activation energies for chemisorption (–0.51 and

–0.44 eV, respectively) and opening of the bandgap to a range of 82–95 meV.[172]

Spintronics: Spintronics is an exciting and potentially revolutionary field that utilizes the spin of an electron to process relevant data, rather than the charge as is the case for conventional electronics. Elemental 2D materials may be the key to future spintronics as the spin lifetimes in these materials are often extended to measureable time scales owing to quantum confinement and long spin–orbit coupling.[173] Of these materials, bismuthene appears to be one of the more exciting as it has been experimentally operated as a topological insulator near room temperature by Reis et al.[26] Other topological insulators only operate at really low temperatures (<4 K) due to the small energy gaps, but the large 0.8 eV energy gap in bismuthene, attributed to the high-atomic number element and enhanced spin–orbit coupling, can enable detectable spin currents. Puckered allotrope of bismuth (Bi (110)) has also been reported to possess 2D topological insulating behavior in 2 and 4 monolayers, which is sensitive to atomic buckling, which in turn could be controlled by choosing different substrates for Bi (110) growth.[53] Other elemental 2D materials such as silicene and stanene have been discussed as new and emerging spintronic materials. Stanene has been predicted to exhibit a large-gap quantum spin gap of 0.3 eV, which could enable room temperature spintronics similar to those hypothesized in bismuthene.[80] More recently, development in the elemental plumbene have shown an even larger energy gap of 400 meV, which is greater than that of the other group IV materials, namely graphene (10^{-3} meV), silicene (8 meV), germanene (23 meV), and stanene (300 meV), approaching the energies needed for room temperature spintronics.[103,107,174,175] Plumbene is predicted to become a topological insulator with a large bulk gap of 200 meV through electronic doping, which is robust to externally applied strain.[107] More experimental work is needed to realize and test the feasibility and reliability of these spintronic devices, but the mounting theoretical evidence suggests potential technology revolutions in spintronics based on elemental 2D materials.

While elemental 2D materials inherently exhibit many exciting properties that make them strong candidates for future electronic and sensors, combining these materials in the form of heterostructures can further enable coupled or enhanced effects that the materials do not exhibit individually. For instance, experimental lateral heterostructures were recently fabricated from borophene/perylenetetracarboxylic dianhydride (PTCDA), demonstrating metal/semiconductor behavior and resistive switching due to the abrupt borophene/polymer interfaces.[176] The transition in density of states from borophene to PTCDA occurred at the molecular length scale because of these sharp interfaces. Understanding interfacial, excitonic and electronic properties of these heterostructures with elemental 2D materials is an exciting field of research still to be explored.

7. Photonic and Optoelectronic Applications

As discussed above and shown in Figure 5, a number of elemental 2D materials exhibit semiconducting properties, and hence can emit photons via recombination of excitons (electron–hole pairs).[177] This emission is thickness dependent and can be tuned by doping or by applying external stimuli (strain). Moreover, the puckered or buckled structures of elemental 2D materials lead to anisotropy in the optical conductivity, which allow a new degree of freedom for designing conceptually new optoelectronic and electronic devices that are not possible using conventional or other 2D materials. Below we describe progress in three application areas in photonics and optoelectronics where 2D materials are heavily being investigated.

Plasmonics: Plasmons are collective charge oscillations that occur in solids in through Coulomb interactions. While the plasmons in semiconducting 2D materials (graphene, phosphorene, and so on) appear in the mid/near-infrared frequency range (and generally only upon doping), plasmons in intrinsically metallic 2D materials such as borophene can extend into the visible range due to their higher carrier concentrations.[45] In addition, the plasmon dispersion in 2D materials is affected heavily by structural anisotropy (as in the case of buckled and puckered 2D materials), electron density, spin–orbit interaction and strain; in-depth reviews on plasmonic properties of several 2D materials can be found elsewhere.[178–180] An example of how structural anisotropy affects the plasmon dispersion is shown in **Figure 7**a. Phosphorene exhibits anisotropic electron masses depending on the crystal orientation, with the electron mass higher (lower) along the zigzag (armchair) direction. As a consequence, the plasmon frequency along the zigzag direction ($\Gamma - Y$ in the Brillouin zone) is higher than the armchair direction ($\Gamma - X$). These dispersions can be changed by applying biaxial strain resulting in a reversal in the plasmon frequency.[181] Phosphorene-based devices can therefore be used in anisotropic plasmonic devices where strain or light polarization induces changes in the device response.[182] Surface plasmons in 2D materials strongly couple with light, creating waves termed surface plasmon polaritons (SPP). Huber et al. demonstrated ultrafast switches on the fs time scale by making phosphorene/SiO_2 heterostructures wherein the surface phonon modes of SiO_2 hybridize with surface plasmons in phosphorene. This occurs upon irradiation with mid-IR light as the interband excitation source, which creates the hybrid interface polariton. As shown in Figure 7b, the ultrafast switching of these polaritons can be used for digital logic circuits involving nanophotonic devices. Finally, an emerging application involving plasmons is thermoplasmonics, where light irradiation coupled to surface plasmons can cause localized hotspots. This technique is particularly useful for photothermal treatments in medicine, and has been successfully demonstrated for removing tumors in mice.[183]

Photodetectors: One of the first optoelectronic applications targeted for 2D materials was photodetection. Semiconducting 2D materials have bandgaps ranging from visible to infrared wavelengths, making them ideally suited for broadband photodetection.[185,201–203] Current photodetection technology is primarily based on silicon with its high performance, low cost, maturity, and high level of integration with electronics. However, applications involving photodetection in the infrared, i.e., below the bandgap of Si (1.1 eV) rely on more exotic semiconductors such as InGaAs or HgCdTe.[185] Of particular interest is the detection of wavelengths centered ≈1.55 μm, the so-called telecom band (C-band, ranging from

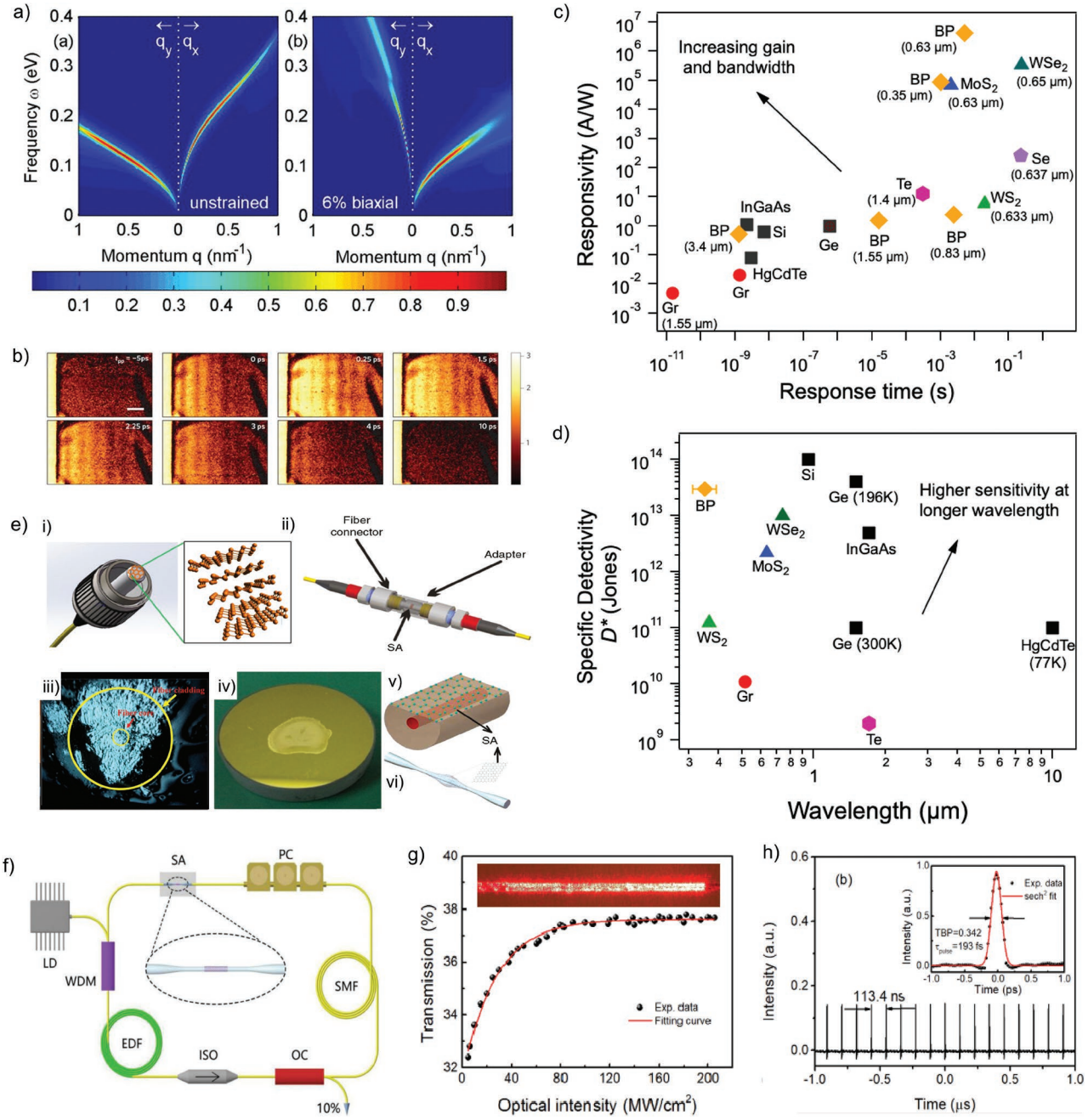

Figure 7. Photonics and optoelectronics applications of elemental 2D materials. a) Plasmon dispersion of phosphorene in the unstrained (left) and strained (right) states, showing strong anisotropy along the armchair and zigzag directions. Reproduced with permission.[181] Copyright 2015, AIP Publishing. b) Scattered near-field intensity images of the black phosphorus/SiO_2 heterostructure, plotted for eight different delay times between the pump and probe pulses (Scale bar 1 μm). The interference fringes indicate motion of the polariton across the interface. Reproduced with permission.[184] Copyright 2016, Springer Nature. c) Various 2D-material-based photodetector technologies plotted against their corresponding responsivity and time response. The top left region corresponds to high gain and high bandwidth detectors and should be the ultimate performance target of future technologies. Data from refs. [28,185–193]. d) Plot of the specific detectivity D^* of various photodetectors versus detected wavelength. Data from refs. [191,193–196]. e) Integration schemes for 2D-material-based saturable absorbers, showing: i) a schematic of black phosphorus coated fiber end and ii) its assembly into the photonic circuit through an adapter. e-i,ii) Reproduced with permission.[197] Copyright 2015, American Chemical Society. iii) A black-phosphorus-coated fiber end. Reproduced with permission.[198] Copyright 2015, Optical Society of America. iv) Gold electrode. e-iii,iv) Reproduced under the terms of the CC-BY Creative Commons Attribution 4.0 International License (http://creativecommons.org/licenses/by/4.0/).[199] Copyright 2016, The Authors, published by Springer Nature. v) 2D materials coated on D-shaped fiber, and vi) embedded on a microfiber. e-v,vi) Reproduced under the terms of the CC-BY Creative Commons Attribution 4.0 International License (http://creativecommons.org/licenses/by/4.0/).[200] Copyright 2016, Springer Nature. f) Experimental setup of an ultrafast fiber laser using bismuthene as the saturable absorber. The components include a continuous wavelength pump laser diode (LD), wavelength-division multiplexer (WDM), erbium-doped, and single-mode fibers (EDF and SMF), polarization isolator (ISO) and controller (PC), optical coupler (OC), and the saturable absorber (SA). g) Nonlinear saturable absorption curve of the microfiber-based bismuthene device (Inset: its corresponding red light image), h) pulse train output of the laser at 250 mW. f–h) Reproduced with permission.[192] Copyright 2018, Optical Society of America.

1.53 to 1.57 μm) most commonly used for fiber optic communications, i.e., around which optical fibers exhibit the lowest loss. 2D materials, including graphene, transition metal dichalcogenides, and elemental materials have bandgaps that span this wavelength range, from near IR (NIR) to mid-IR (MIR) and far-IR (FIR), i.e., 1 to 10 μm, and are emerging candidates for such IR detectors. In terms of performance, the ideal photodetector must exhibit high responsivity (typically measured in A W^{-1}) and low response time (or high frequency bandwidth) as well as a high specific detectivity.[185] This figure of merit, labeled D^* is measured as the reciprocal of the noise equivalent power (NEP) normalized per square root of the sensor area and frequency bandwidth and commonly expressed in the Jones units (cm$\sqrt{\text{Hz}}$ W^{-1}).

One of the most heavily studied elemental materials for photodetectors is phosphorene, a direct gap semiconductor with bandgaps ranging from 0.3 eV in the bulk up to ≈2 eV for a monolayer. This range allows for the detection of radiation from ≈600 nm up to ≈4 μm; photodetectors based on multilayer phosphorene have been demonstrated at a variety of wavelengths ranging from 350 nm up to 3.4 μm.[188,189,204–206] However, the oxidative stability of phosphorene remains an on-going issue that must be addressed to realize large-scale applicability in IR photodetectors. In addition to phosphorene, other elemental materials such as tellurene and selenene have also been studied as photodetectors in the IR and visible region, respectively. Figure 7c,d summarizes the photodetector performance and figures of merit for several elemental 2D materials. Also plotted in Figure 7c,d are values for commercial materials (Si, Ge, InGaAs, and HgCdTe) as well as other 2D materials including graphene and transition metal dichalcogenides (MoS_2, WS_2, and WSe_2). Figure 7c shows that in general the responsivity of 2D-material-based photodetectors is as high (0.1–1 A W^{-1}) or even higher (up to 10^7 A W^{-1}) than traditional materials. However, the average response times are much slower (ms rather than ns timescales) due to a number of factors such as photogating, device architecture as well as trapped charges at interfaces and defects.[207] Future improvements in device performance should result in lower response times (higher bandwidths) and higher responsivities. The specific detectivity (D^*) of several 2D materials at their wavelength of detection is plotted in Figure 7d. Many studied 2D materials have specific detectivity on par or lower than the D^* in existing photodetector materials. Present and future research efforts could help towards increasing the D^* at longer wavelengths, IR for instance. Moreover, due to the difficulty in synthesizing elemental 2D material such as borophene, silicene, germanene, and stanene, their efficacy as photodetector materials remains to be studied and further explored.

Ultrafast Lasers: Fiber-based ultrafast lasers typically employ mode-locking technology whereby a continuous-wavelength laser is converted into a pulsed laser. This is done using a saturable absorber (SA), a nonlinear optical material whose light absorption decreases with increasing intensity. The ideal SA has good absorption properties (its transmittance increases with increasing input laser fluence), low mode-locking threshold, high damage threshold, broad working wavelength range, and short recovery time. Current commercial ultrafast lasers employ semiconducting saturable absorber mirrors (SESAMs), a quantum-well structure prepared by MBE. SESAM-based SAs are difficult to fabricate, expensive, and have a narrow operating wavelength range.[208] These limitations have prompted the search for alternate materials such as graphene and carbon nanotubes as SAs.[209] More recently, 2D materials with their wide range of optical properties (absorption ranges and bandgaps) have also emerged as promising candidates for SAs in ultrafast lasers.[210–213] In addition to their optical properties, the layered nature of 2D materials makes it easy to coat ultrathin films on to optical elements for integration into laser systems. Figure 7e depicts the integration of 2D materials as SAs into ultrafast laser setups. The 2D materials can be directly coated on to the open end of a fiber, or on to an adapter between two fibers (Figure 7e-i,ii). Figure 7e-iii,iv shows two examples of phosphorene SAs coated as a thick film on a fiber end and as a thin film on a gold electrode, respectively. Other integration schemes involve coating of 2D materials on D-shaped fibers or tapered microfibers (Figure 7-ev,vi).

Other than graphene, one of the first elemental 2D materials to be studied as a SA was phosphorene,[198,214–220] which has been demonstrated as a good candidate for nonlinear absorption over a broad wavelength range (1–3 μm) and used in mode-locked and Q-switched lasers.[221] While black phosphorus has shown excellent nonlinear optical properties as SAs, its instability under ambient conditions hinders widespread use in ultrafast lasers; various passivation schemes have been studied for improving device performance.[158,222] Other elemental 2D materials such as bismuthene have recently been investigated as alternatives to phosphorene. In addition to having excellent mechanical properties, bismuthene is a narrow bandgap semiconductor and is stable at high temperatures.[52] Few layer bismuthene has been used as SAs in mode-locked fiber lasers, producing stable fs pulses ≈1550 nm.[192,223,224] Among other group V elements, antimonene has also been used as an SA in passive Q-switched lasers and shown stable ns pulse widths for laser emission at 946, 1064, and 1342 nm.[225] As the synthesis of other elemental materials such as silicene, germanene, stanene, and borophene matures, we can also expect to see them being used as SAs in ultrafast lasers.

8. Power and Energy

Future power and energy systems will rely on robust, reliable, and highly efficient strategies that deliver, store, and transmit power to global communities. In this section, we address how the exceptional properties of elemental 2D materials are expected to play a role in new technologies for such systems and discuss the relevant literature to date.

Batteries: In order to power future electronics and consumer devices, batteries must increase their gravimetric and volumetric storage capacities. At the same time, the miniaturization of electronics and the recent focus on flexible and wearable electronics necessitates the development of light-weight energy storage devices without sacrificing performance. In this regard, 2D materials are attractive candidates as active electrodes in existing and next-generation energy storage devices owing to their form factor and high specific surface areas.

A Li-ion battery consists of two electrodes (anode and cathode) with a separator between them. An ionic electrolyte

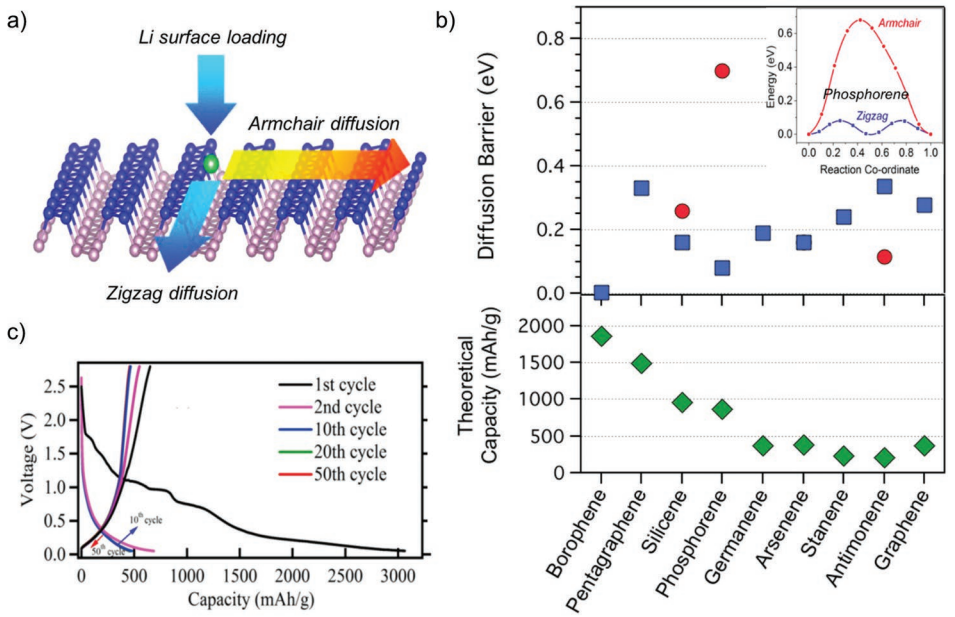

Figure 8. Li-ion battery applications of elemental 2D materials. a) Schematic showing ultrafast Li-ion diffusion along the armchair direction in phosphorene. Reproduced with permission.[226] Copyright 2015, American Chemical Society. b) Theoretical diffusion barriers and Li-ion capacities for several monolayer elemental 2D materials. Data from refs. [227–234]. The inset shows energy profiles of Li diffusion along the armchair and zigzag directions on phosphorene surface. Reproduced with permission.[226] Copyright 2015, American Chemical Society. c) Charge–discharge voltage versus Li-ion capacity curves tested at C/10 rate for phosphorene battery anodes. Reproduced with permission.[230] Copyright 2017, IOP Publishing.

between the two electrodes serves as the medium for diffusion of Li ions. Most current Li ion batteries employ graphite anodes and Li-metal oxide cathodes (e.g., lithium cobalt oxide or LCO). Owing to their anisotropic structures, Li diffusion in elemental 2D materials can be highly directional. For example, Li diffusion is much higher in the armchair direction in phosphorene than zig-zag direction (**Figure 8**a).[226] Similarly, the barriers for Li diffusion along the various crystallographic directions (armchair and zigzag) vary for different 2D material compositions (Figure 8b). Phosphorene exhibits the highest anisotropy among elemental 2D materials, with antimonene and silicene also exhibiting Li diffusion with lower barriers along certain crystallographic directions. Interestingly, this anisotropy does not necessarily correlate to high Li capacity (bottom panel of Figure 8b).

Among elemental 2D materials, borophene exhibits the highest theoretical capacity for Li (≈1860 mAh g^{-1}).[227] Barring stanene and antimonene, the theoretical Li-ion capacities for all elemental 2D materials is higher than for graphene. The large Li-ion capacity of borophene is due to the ultralow diffusion barrier for Li (2.6 meV) and large Li adsorption energy (1.16 eV).[227] The diffusion barrier is very low along the furrows of the borophene lattice (see Figure 2), but much higher (325 meV) in the orthogonal direction. This kind of difference in Li ion diffusion is also present in the puckered structure of phosphorene, where theoretical calculations reveal ultrahigh diffusivity of Li ions along the armchair direction,[226] compared to the zigzag direction. This results in a relatively high Li-ion capacity of 865 mAh g^{-1}.[230] While Li-ion batteries based on borophene have yet to be experimentally realized, multi-layer phosphorene sheets have already demonstrated potential as battery anodes (Figure 8c),[230] although issues such as capacity fading and irreversible loss after the first cycle must be solved for their large-scale applicability.

One concern with Li intercalation in phosphorene sheets (similar to Li intercalation in bulk Si) is that it results in a large volume expansion, as shown by in situ TEM experiments.[235] In spite of this, phosphorene-based anodes have shown to retain their structural integrity upon lithiation and delithiation process. Interestingly, the large volume expansion of bulk Si is mitigated in silicene due to its larger interlayer distance, suggesting that silicene is a better candidate for Li-ion storage than bulk Si.[229] Among the other puckered elemental 2D materials, arsenene also exhibits a high capacity for Li and Na ions (as high as 1072 mAh g^{-1} for Li_3As) and recent experiments employing arsenene/carbon nanocomposite anodes have demonstrated a Li-ion capacity of 1306 mAh g^{-1} (after 100 cycles).[236]

In addition to replacing anodes in Li-ion battery architectures, elemental 2D materials are also attractive candidates for electrodes in next-generation battery technologies such as Li-sulfur and Na-ion batteries. Li-sulfur cathodes offer high specific capacities for Li and S storage and have recently attracted much attention.[237,238] However, they suffer from drawbacks such as low electrical and ionic conductivities of sulfur, high volume change upon lithiation, and loss of sulfur due to dissolution within the electrolyte.[238] Further theoretical and experimental studies have shown that phosphorene is capable of immobilizing undesirable polysulfides, thereby prolonging the lifetime of Li-S batteries.[239]

Na-ion batteries are also being researched heavily as alternatives to Li-ion batteries owing to the relative abundance of Na and potential low cost of fabricating Na-ion batteries.[240] However, the larger size of the Na ion compared to the Li ion (atomic radius 1.16 Å compared to 0.9 Å) and the

thermodynamic instability of NaC_6 and NaC_8 effectively prohibit the use of graphite anodes as Na-ion intercalation media. The buckled and puckered structures of Group V elemental 2D materials are thus particularly attractive for Na-ion intercalation. Among these, arsenic exhibits the highest theoretical capacity for Na-ions (1072 mAh g^{-1})[236] followed by antimony (660 mAh g^{-1}),[241] phosphorus (430 mAh g^{-1}),[242] and bismuth (386 mAh g^{-1}).[243] In addition to the high capacities Na-ion diffusivity is anisotropic along the edges of the puckered structures of the Group V monolayers, and in the case of phosphorene has been predicted to be fastest along the zigzag direction.[242] Recently, few-layer arsenene-based anodes have demonstrated a Na-ion capacity of 750 mAh g^{-1} after 200 cycles, which is lower than the theoretical capacity of As and was attributed to volume expansion.[236] On the other hand, few-layer P anodes exhibited a Na-ion capacity of 453 mAh g^{-1}, close to the theoretical value.[230] The capacity remained stable and reversible over 50 cycles. Few-layer Sb-based batteries have also demonstrated a high capacity of 620 mAh g^{-1} at 0.5C, with a 99.7% retention of capacity over 150 cycles.[244]

Supercapacitors: While rechargeable batteries remain the top choice for energy storage due to their high energy densities, their short cycle life and relatively slow charge/discharge times result in lower power densities. As a result, supercapacitors or ultracapacitors have emerged as attractive alternatives to batteries and offer advantages such as superior lifetimes, higher power densities, and ultrafast charge/discharge rates. Supercapacitors are composed of two electrodes that can collect and store charge through electrostatic ion adsorption (electrical double-layer capacitors, or EDLCs) or through reversible redox reactions (pseudocapacitors). Owing to their form factor, layered 2D materials serve as ideal electrodes, offering high surface areas, high power densities, and high flexibility for EDLCs as well as pseudocapacitors.[245–247] Among elemental 2D materials, phosphorene was one of the first materials studied for use in supercapacitors. A flexible solid-state capacitor based on liquid-phase exfoliated phosphorene nanosheets was reported to have a volumetric capacitance of 17.78 F cm^{-3} (59.3 F g^{-1}) at 0.1 V s^{-1} and 1.43 F cm^{-3} (4.8 F g^{-1}) at 10 V s^{-1}, exhibiting an excellent rate capacitance.[248] Moreover, the supercapacitor had a high capacitance retention (≈71.8%) after 30 000 cycles. Hybrids of black phosphorus with several other materials such as red phosphorus,[249] graphene,[250] polypyrrole[251] have also been reported, exhibiting a wide range of specific and volumetric capacitances. Among other 2D materials, antimonene was recently employed in supercapacitors—screen printed EDLCs with carbon electrodes were fabricated with the addition of antimonene flakes, resulting in a very high specific capacitance (1578 F g^{-1}) at a high current charging density (14 A g^{-1}).[252]

In general, the capacitance in an EDLC depends on contributions from the differential electrochemical double layer as well as the intrinsic quantum capacitance of the electrode, which could limit the overall performance.[253,254] In this regard, a recent theoretical study on silicene suggests that adding vacancies to a silicene monolayer can increase its quantum capacitance significantly (by an order of magnitude).[255] This offers a path forward to designing better supercapacitors through defect engineering. Such approaches could also help address one of the biggest drawbacks of supercapacitors, which is their lower energy density compared to batteries.[256] Another drawback of 2D materials is restacking of layers after exfoliation, lowering the number of sites available for charge accumulation; future studies can improve on device architectures to enable efficient charge insertion and extraction.

Thermoelectrics: Elemental 2D materials also can play a role in the formation of new and novel thermoelectronic devices, as strategies such as nanostructuring and lowered dimensionalities from bulk to 2D or 1D morphologies can influence the thermal and electrical conductivities (by increasing electron confinement and phonon scattering) in a thermoelectric material.[257–260] Bi- and Sb-based materials have traditionally been the best thermoelectric materials, and their buckled and puckered structures could provide attractive alternatives for next-generation thermoelectrics.

The structural anisotropy in the layers of the Group V elements results in anisotropic thermal conductivity along certain preferred directions. For example, it is predicted that thermal transport in the armchair direction is much lower than the zigzag direction in antimonene,[261] arsenene,[262] and phosphorene.[263] This anisotropic thermal transport, coupled with the buckled or puckered structure in the monolayers leads to very low thermal conductivities due to high anharmonicity, as in layered SnSe.[264,265] Ab initio calculations in combination with the Boltzmann transport equation for phonons show that antimonene has a low lattice thermal conductivity (15.1 W m^{-1} K^{-1} at 300 K), indicating its potential thermoelectric applications.[266] Carrete et al. calculated the thermal conductivity of a few different arsenene structures, i.e., buckled, puckered, and square, and room temperature values range from ≈2.5 to ≈7 W m^{-1} K^{-1}, with the highest thermal conductivity in the zigzag direction.[262] In phosphorene, the thermal conductivities along the armchair and zigzag direction have been calculated to be 13 and 30 W m^{-1} K^{-1}, respectively.[267] These thermal conductivity values are on par with those found in traditional bulk thermoelectric materials (typically <5 W m^{-1} K^{-1}).[268]

Importantly, the reduced dimensionality of buckled and puckered group V monolayers also results in changes in the other factors that affect ZT, namely electrical conductivity and Seebeck coefficient. First principles calculations show that lattice electrical and thermal conductivities are orthogonal to each other in phosphorene[269] and arsenene,[270] thereby enhancing the ratio between the two values and maximizing the *ZT*. Recent theoretical studies predict high *ZT* values approaching 2.1 at 300 K[261] in buckled antimonene and 2.1 and 2.4 at 300 K[271] for n- and p-doped bismuthene, respectively. The *ZT* is predicted to be higher for applied strain as well as higher doping concentrations. Moreover, novel morphologies such as nanoribbons with preferred edges along their long axes could further enhance thermoelectric figure of merit by decoupling the thermal and electronic contributions to ZT.

9. Outlook and Conclusions

Over 15 different 2D elemental analogues of main group elements have been experimentally and theoretically explored for a variety of novel applications. **Figure 9** (top) shows the current status of such reported literature as a correlation between the

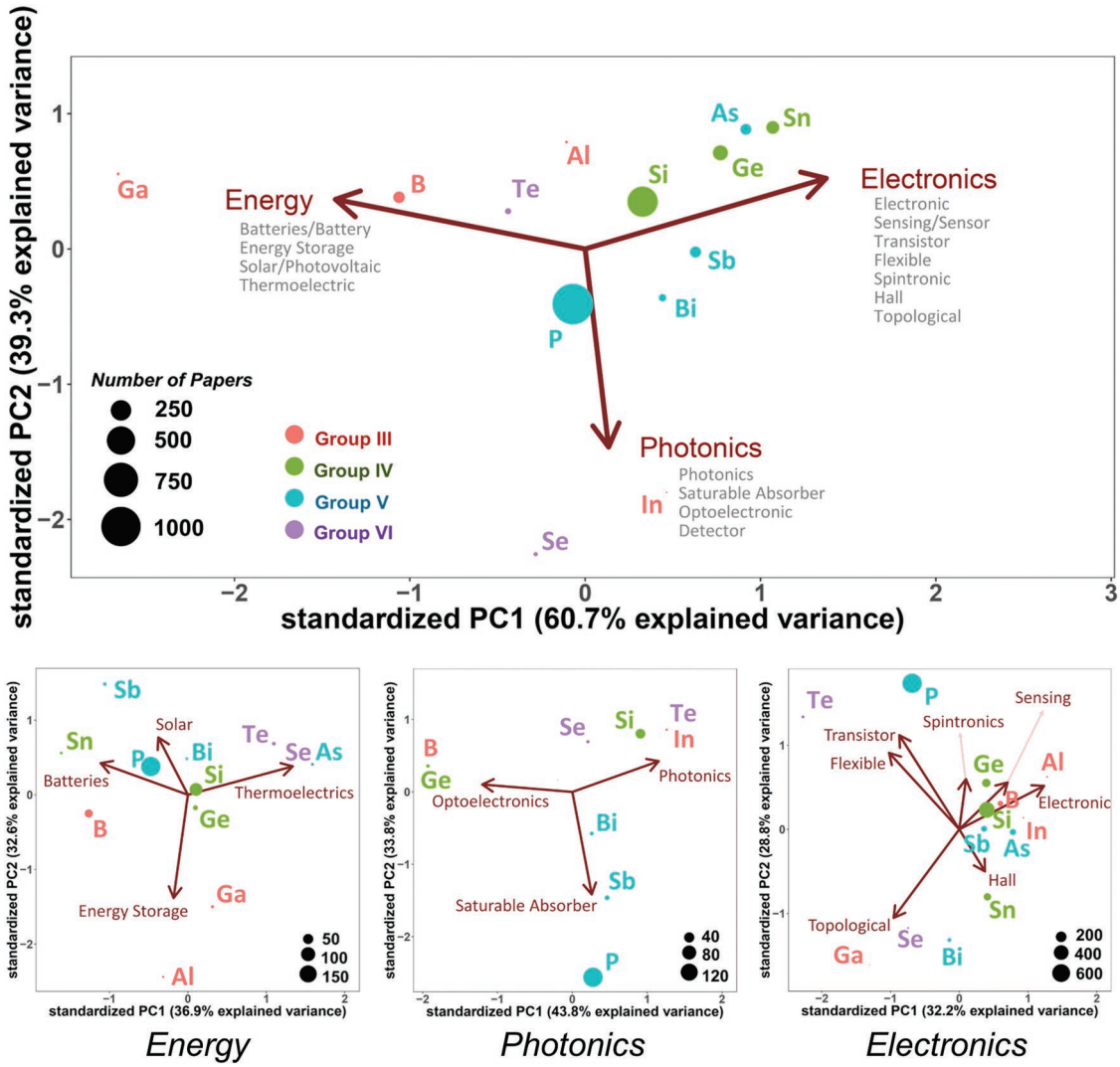

Figure 9. PCA analysis of applications for elemental 2D materials.

elements and their reported applications in the broad area of electronics, energy, and photonics (specific search keywords on Google Scholar corresponding to words in the manuscript titles are listed below the application names) in a principal component analysis plot. It can be seen that for the three studied applications variables, the first two principal components can explain all the variance in the data. Several key concepts can be obtained from Figure 9 that can help guide future research efforts. First, while phosphorene and silicene are well studied to date (as represented by their symbol size), elements such as gallinene, indiene, aluminene, and plumbene are in their research infancy. Second, there is no observable correlation among the applications as variable vectors (applications) as they are almost equiangular from each other. Third, the specific location of elemental data point on the PCA plot provides an insight into what exists in the current literature for that particular element (in terms of applications) and where are the next opportunities. For example, if the data point sits at origin, there are equal number of reported studies in each of the three investigated application categories. From the plot, one can see that most of the research of moderately to well-studied elemental 2D materials (arsenene, antimonene, germanene, stanene, and silicene) have been driven toward electronic applications, suggesting an opportunity to explore their potential in energy and optoelectronics applications to a greater degree. Similarly, materials that are still in their research infancy such as gallinene, indiene, and selenene are located toward one of the application vectors, which indicates that most of the handful of studies have focused on one application aspect of that element. In such cases, there exists extensive opportunities to continue building a knowledge database in that application as well as explore other applications. Figure 9 (bottom) further breaks down the state of the current literature for each specific application area. A similar analysis can be made for sub-application areas (using the listed search keywords) in terms of current application space that has been explored to date and where the future opportunity space is.

Technological revolutions built around elemental 2D materials will require a significant amount of research, engineering, and development in the coming years. First, synthesis

of elemental 2D materials must be better understood at a fundamental level and developed to ensure reliability during large-scale production, which may be easier for monoelemental materials than some of the more chemically complicated 2D materials such as transition metal dichalcogenidess and MXenes. Future synthesis strategies must be tailored to the application of interest, with lower cost, more scalable techniques for applications such as flexible electronics and batteries, and high fidelity, reliable techniques for applications such as plasmonics, photodetectors, and spintronics. Second, the long-term environmental stability and strategies to mitigate degradation of the materials must be taken into consideration depending on the particular application. For example, a gas sensor based on black phosphorous will need to physically interact with the environment by respond to any adsorbed molecular while also ensuring device longevity. Third, predicted properties of elemental 2D materials (such as ferroelectricity[46]) that are unexplored may be key to unlocking another gamut of future applications. The exciting and revolutionary properties need to be not just "one off" experiments but evaluated from a statistical approach to determine the viability and accessibility of these properties on a commercial scale. Finally, in order for elemental 2D materials (and 2D materials in general) to truly create a stronghold in the consumer market, the benefits of 2D materials relative to the 3D counterpart need to be explicitly defined. Taking advantage of the opportunities that nanoscale materials exhibit such as high surface to volume ratio, long spin lifetimes, and high storage capacities will require overwhelming evidence to support commercialization over more mature 3D materials. However, despite the significant challenges ahead, there is no doubt that the exceptional properties of these exciting materials will influence the future technology space in applications such as nanoelectronics, sensing, spintronics, photonics, thermoelectrics, and energy systems.

Supporting Information

Supporting Information is available from the Wiley Online Library or from the author.

Acknowledgements

N.G. thanks the support of Air Force Office of Scientific Research grant FA9550-19RYCOR050. E.R. acknowledges support from the Air Force Office of Scientific Research Young Investigator Program FA9550-17-1-0202. P.A. acknowledges support from the Air Force Office of Scientific Research under FA9550-18-1-0072.

Conflict of Interest

The authors declare no conflict of interest.

Keywords

2D materials, applications of 2D materials, elemental 2D materials

Received: July 5, 2019
Revised: August 8, 2019
Published online: October 31, 2019

[1] I. Langmuir, C. G. Suits, *The Collected Works of Irving Langmuir: Surface Phenomena*, Pergamon Press, Oxford, UK **1961**.
[2] J. P. Biberian, G. A. Somorjai, *J. Vac. Sci. Technol.* **1979**, *16*, 2073.
[3] K. S. Novoselov, A. K. Geim, S. V. Morozov, D. Jiang, *Science* **2004**, *306*, 666.
[4] M. Naguib, V. N. Mochalin, M. W. Barsoum, Y. Gogotsi, *Adv. Mater.* **2014**, *26*, 992.
[5] A. J. Mannix, B. Kiraly, M. C. Hersam, N. P. Guisinger, *Nat. Rev. Chem.* **2017**, *1*, 0014.
[6] S. Z. Butler, S. M. Hollen, L. Cao, Y. Cui, J. A. Gupta, H. R. Gutierrez, T. F. Heinz, S. S. Hong, J. Huang, A. F. Ismach, E. Johnston-Halperin, M. Kuno, V. V. Plashnitsa, R. D. Robinson, R. S. Ruoff, S. Salahuddin, J. Shan, L. Shi, M. G. Spencer, M. Terrones, W. Windl, J. E. Goldberger, *ACS Nano* **2013**, *7*, 2898.
[7] X. Xiao, H. Song, S. Lin, Y. Zhou, X. Zhan, Z. Hu, Q. Zhang, J. Sun, B. Yang, T. Li, L. Jiao, J. Zhou, J. Tang, Y. Gogotsi, *Nat. Commun.* **2016**, *7*, 11296.
[8] M. Z. Hasan, C. L. Kane, *Rev. Mod. Phys.* **2010**, *82*, 3045.
[9] C. L. Kane, E. J. Mele, *Phys. Rev. Lett.* **2005**, *95*, 226801.
[10] M. König, S. Wiedmann, C. Brüne, A. Roth, H. Buhmann, L. W. Molenkamp, X.-L. Qi, S.-C. Zhang, *Science* **2007**, *318*, 766.
[11] A. S. Mayorov, R. V. Gorbachev, S. V. Morozov, L. Britnell, R. Jalil, L. A. Ponomarenko, P. Blake, K. S. Novoselov, K. Watanabe, T. Taniguchi, A. K. Geim, *Nano Lett.* **2011**, *11*, 2396.
[12] K. S. Novoselov, A. K. Geim, S. V. Morozov, D. Jiang, M. I. Katsnelson, I. V. Grigorieva, S. V. Dubonos, A. A. Firsov, *Nature* **2005**, *438*, 197.
[13] J. R. Schaibley, H. Yu, G. Clark, P. Rivera, J. S. Ross, K. L. Seyler, W. Yao, X. Xu, *Nat. Rev. Mater.* **2016**, *1*, 16055.
[14] Q. H. Wang, K. Kalantar-Zadeh, A. Kis, J. N. Coleman, M. S. Strano, *Nat. Nanotechnol.* **2012**, *7*, 699.
[15] T. Mueller, E. Malic, *npj 2D Mater. Appl.* **2018**, *2*, 29.
[16] K. S. Novoselov, A. Mishchenko, A. Carvalho, A. H. Castro Neto, *Science* **2016**, *353*, aac9439.
[17] A. Castellanos-Gomez, *Nat. Photonics* **2016**, *10*, 202.
[18] B. Aufray, A. Kara, S. Vizzini, H. Oughaddou, C. Léandri, B. Ealet, G. L. Lay, *Appl. Phys. Lett.* **2010**, *96*, 183102.
[19] L. Li, Y. Yu, G. J. Ye, Q. Ge, X. Ou, H. Wu, D. Feng, X. H. Chen, Y. Zhang, *Nat. Nanotechnol.* **2014**, *9*, 372.
[20] M. E. Dávila, L. Xian, S. Cahangirov, A. Rubio, G. Le Lay, *New J. Phys.* **2014**, *16*, 095002.
[21] S. Zhang, Z. Yan, Y. Li, Z. Chen, H. Zeng, *Angew. Chem., Int. Ed.* **2015**, *54*, 3112.
[22] F.-F. Zhu, W.-J. Chen, Y. Xu, C.-L. Gao, D.-D. Guan, C.-H. Liu, D. Qian, S.-C. Zhang, J.-J. Jia, *Nat. Mater.* **2015**, *14*, 1020.
[23] A. J. Mannix, X.-F. Zhou, B. Kiraly, J. D. Wood, D. Alducin, B. D. Myers, X. Liu, B. L. Fisher, U. Santiago, J. R. Guest, M. J. Yacaman, A. Ponce, A. R. Oganov, M. C. Hersam, N. P. Guisinger, *Science* **2015**, *350*, 1513.
[24] T. Lei, C. Liu, J.-L. Zhao, J.-M. Li, Y.-P. Li, J.-O. Wang, R. Wu, H.-J. Qian, H.-Q. Wang, K. Ibrahim, *J. Appl. Phys.* **2016**, *119*, 015302.
[25] D. Singh, S. K. Gupta, I. Luka čević, Y. Sonvane, *RSC Adv.* **2016**, *6*, 8006.
[26] F. Reis, G. Li, L. Dudy, M. Bauernfeind, S. Glass, W. Hanke, R. Thomale, J. Schäfer, R. Claessen, *Science* **2017**, *357*, 287.
[27] Z. Zhu, X. Cai, S. Yi, J. Chen, Y. Dai, C. Niu, Z. Guo, M. Xie, F. Liu, J. H. Cho, Y. Jia, Z. Zhang, *Phys. Rev. Lett.* **2017**, *119*, 106101.
[28] J. Qin, G. Qiu, J. Jian, H. Zhou, L. Yang, A. Charnas, D. Y. Zemlyanov, C. Y. Xu, X. Xu, W. Wu, H. Wang, P. D. Ye, *ACS Nano* **2017**, *11*, 10222.
[29] V. Kochat, A. Samanta, Y. Zhang, S. Bhowmick, P. Manimunda, S. A. S. Asif, A. S. Stender, R. Vajtai, A. K. Singh, C. S. Tiwary, P. M. Ajayan, *Sci. Adv.* **2018**, *4*, e1701373.
[30] J. Yuhara, B. He, N. Matsunami, M. Nakatake, G. Le Lay, *Adv. Mater.* **2019**, *31*, 1901017.

[31] K. H. Yeoh, T. L. Yoon, Rusi, D. S. Ong, T. L. Lim, *Appl. Surf. Sci.* **2018**, *445*, 161.
[32] J. Nevalaita, P. Koskinen, *Phys. Rev. B* **2018**, *97*, 035411.
[33] H.-S. Tsai, S.-W. Wang, C.-H. Hsiao, C.-W. Chen, H. Ouyang, Y.-L. Chueh, H.-C. Kuo, J.-H. Liang, *Chem. Mater.* **2016**, *28*, 425.
[34] B. Peng, H. Zhang, H. Shao, Z. Ning, Y. Xu, G. Ni, H. Lu, D. W. Zhang, H. Zhu, *Mater. Res. Lett.* **2017**, *5*, 399.
[35] J. Yuan, N. Yu, K. Xue, X. Miao, *Appl. Surf. Sci.* **2017**, *409*, 85.
[36] F. Matusalem, M. Marques, L. K. Teles, F. Bechstedt, *Phys. Rev. B* **2015**, *92*, 4.
[37] S. Zhang, J. Zhou, Q. Wang, X. Chen, Y. Kawazoe, P. Jena, *Proc. Natl. Acad. Sci. USA* **2015**, *112*, 2372.
[38] Z. Wang, X.-F. Zhou, X. Zhang, Q. Zhu, H. Dong, M. Zhao, A. R. Oganov, *Nano Lett.* **2015**, *15*, 6182.
[39] L. Xian, A. Pérez Paz, E. Bianco, P. M. Ajayan, A. Rubio, *2D Mater.* **2017**, *4*, 041003.
[40] M. E. Bachra, H. Zaari, A. Benyoussef, A. E. Kenz, A. G. E. Hachimi, *J. Supercond. Novel Magn.* **2018**, *31*, 2579.
[41] B. v. d. Broek, M. Houssa, E. Scalise, G. Pourtois, V. V. Afanas'ev, A. Stesmans, *2D Mater.* **2014**, *1*, 021004.
[42] J. Yuhara, Y. Fujii, K. Nishino, N. Isobe, M. Nakatake, L. Xian, A. Rubio, G. Le Lay, *2D Mater.* **2018**, *5*, 025002.
[43] O. Rahaman, B. Mortazavi, A. Dianat, G. Cuniberti, T. Rabczuk, *FlatChem* **2017**, *1*, 65.
[44] M. Shahrokhi, *Optik* **2017**, *136*, 205.
[45] Y. Huang, S. N. Shirodkar, B. I. Yakobson, *J. Am. Chem. Soc.* **2017**, *139*, 17181.
[46] C. Xiao, F. Wang, S. A. Yang, Y. Lu, Y. Feng, S. Zhang, *Adv. Funct. Mater.* **2018**, *28*, 1707383.
[47] J.-S. Kim, Y. Liu, W. Zhu, S. Kim, D. Wu, L. Tao, A. Dodabalapur, K. Lai, D. Akinwande, *Sci. Rep.* **2015**, *5*, 8989.
[48] Y. Abate, D. Akinwande, S. Gamage, H. Wang, M. Snure, N. Poudel, S. B. Cronin, *Adv. Mater.* **2018**, *30*, 1704749.
[49] Y. Y. Illarionov, M. Waltl, G. Rzepa, J.-S. Kim, S. Kim, A. Dodabalapur, D. Akinwande, T. Grasser, *ACS Nano* **2016**, *10*, 9543.
[50] X. Wu, Y. Shao, H. Liu, Z. Feng, Y.-L. Wang, J.-T. Sun, C. Liu, J.-O. Wang, Z.-L. Liu, S.-Y. Zhu, Y.-Q. Wang, S.-X. Du, Y.-G. Shi, K. Ibrahim, H.-J. Gao, *Adv. Mater.* **2017**, *29*, 1605407.
[51] G. Wang, R. Pandey, S. P. Karna, *ACS Appl. Mater. Interfaces* **2015**, *7*, 11490.
[52] E. Aktürk, O. Uzengi Aktürk, S. Ciraci, *Phys. Rev. B* **2016**, *94*, 014115.
[53] Y. Lu, W. Xu, M. Zeng, G. Yao, L. Shen, M. Yang, Z. Luo, F. Pan, K. Wu, T. Das, P. He, J. Jiang, J. Martin, Y. P. Feng, H. Lin, X.-S. Wang, *Nano Lett.* **2015**, *15*, 80.
[54] J. Lu, Y. Xie, F. Xu, L. Zhu, *J. Mater. Chem.* **2002**, *12*, 2755.
[55] A. Apte, E. Bianco, A. Krishnamoorthy, S. Yazdi, R. Rao, N. Glavin, H. Kumazoe, V. Varshney, A. Roy, F. Shimojo, E. Ringe, R. K. Kalia, A. Nakano, C. S. Tiwary, P. Vashishta, V. Kochat, P. M. Ajayan, *2D Mater.* **2018**, *6*, 015013.
[56] C. Liu, T. Hu, Y. Wu, H. Gao, Y. Yang, W. Ren, *J. Phys.: Condens. Matter* **2019**, *31*, 235702.
[57] D. Chiappe, C. Grazianetti, G. Tallarida, M. Fanciulli, A. Molle, *Adv. Mater.* **2012**, *24*, 5088.
[58] P. Bampoulis, L. Zhang, A. Safaei, R. van Gastel, B. Poelsema, H. J. Zandvliet, *J. Phys.: Condens. Matter* **2014**, *26*, 442001.
[59] M. Derivaz, D. Dentel, R. Stephan, M. C. Hanf, A. Mehdaoui, P. Sonnet, C. Pirri, *Nano Lett.* **2015**, *15*, 2510.
[60] L. Li, S. Z. Lu, J. Pan, Z. Qin, Y. Q. Wang, Y. Wang, G. Y. Cao, S. Du, H. J. Gao, *Adv. Mater.* **2014**, *26*, 4820.
[61] P. Vogt, P. De Padova, C. Quaresima, J. Avila, E. Frantzeskakis, M. C. Asensio, A. Resta, B. Ealet, G. Le Lay, *Phys. Rev. Lett.* **2012**, *108*, 155501.
[62] P. De Padova, O. Kubo, B. Olivieri, C. Quaresima, T. Nakayama, M. Aono, G. Le Lay, *Nano Lett.* **2012**, *12*, 5500.
[63] A. J. Mannix, B. Kiraly, B. L. Fisher, M. C. Hersam, N. P. Guisinger, *ACS Nano* **2014**, *8*, 7538.
[64] M. De Crescenzi, I. Berbezier, M. Scarselli, P. Castrucci, M. Abbarchi, A. Ronda, F. Jardali, J. Park, H. Vach, *ACS Nano* **2016**, *10*, 11163.
[65] L. Zhang, P. Bampoulis, A. N. Rudenko, Q. Yao, A. van Houselt, B. Poelsema, M. I. Katsnelson, H. J. Zandvliet, *Phys. Rev. Lett.* **2016**, *116*, 256804.
[66] T. P. Kaloni, U. Schwingenschlögl, *J. Appl. Phys.* **2013**, *114*, 184307.
[67] B. Feng, J. Zhang, Q. Zhong, W. Li, S. Li, H. Li, P. Cheng, S. Meng, L. Chen, K. Wu, *Nat. Chem.* **2016**, *8*, 563.
[68] L. Tao, E. Cinquanta, D. Chiappe, C. Grazianetti, M. Fanciulli, M. Dubey, A. Molle, D. Akinwande, *Nat. Nanotechnol.* **2015**, *10*, 227.
[69] M. E. Dávila, G. Le Lay, *Sci. Rep.* **2016**, *6*, 20714.
[70] J. Deng, B. Xia, X. Ma, H. Chen, H. Shan, X. Zhai, B. Li, A. Zhao, Y. Xu, W. Duan, S.-C. Zhang, B. Wang, J. G. Hou, *Nat. Mater.* **2018**, *17*, 1081.
[71] H. Liu, A. T. Neal, Z. Zhu, Z. Luo, X. Xu, D. Tománek, P. D. Ye, *ACS Nano* **2014**, *8*, 4033.
[72] F. Xu, B. Ge, J. Chen, A. Nathan, L. L. Xin, H. Ma, H. Min, C. Zhu, W. Xia, Z. Li, S. Li, K. Yu, L. Wu, Y. Cui, L. Sun, Y. Zhu, *2D Mater.* **2016**, *3*, 025005.
[73] J. Ji, X. Song, J. Liu, Z. Yan, C. Huo, S. Zhang, M. Su, L. Liao, W. Wang, Z. Ni, *Nat. Commun.* **2016**, *7*, 13352.
[74] Y. Aierken, O. Leenaerts, F. M. Peeters, *Phys. Rev. B* **2016**, *94*, 155410.
[75] X. Fan, J. Li, G. Chen, *RSC Adv.* **2017**, *7*, 17417.
[76] J.-W. Jiang, J. Leng, J. Li, Z. Guo, T. Chang, X. Guo, T. Zhang, *Carbon* **2017**, *118*, 370.
[77] X. Li, Q. Wang, P. Jena, *J. Phys. Chem. Lett.* **2017**, *8*, 3234.
[78] G. Long, Y. Zhou, M. Jin, B. Kan, Y. Zhao, A. Gray-Weale, D.-e. Jiang, Y. Chen, Q. Zhang, *Carbon* **2015**, *95*, 1033.
[79] C. P. Ewels, X. Rocquefelte, H. W. Kroto, M. J. Rayson, P. R. Briddon, M. I. Heggie, *Proc. Natl. Acad. Sci. USA* **2015**, *112*, 15609.
[80] Y. Xu, B. Yan, H.-J. Zhang, J. Wang, G. Xu, P. Tang, W. Duan, S.-C. Zhang, *Phys. Rev. Lett.* **2013**, *111*, 136804.
[81] S. Rachel, M. Ezawa, *Phys. Rev. B* **2014**, *89*, 195303.
[82] S. Saxena, R. P. Chaudhary, S. Shukla, *Sci. Rep.* **2016**, *6*, 31073.
[83] C. Kamal, A. Chakrabarti, M. Ezawa, *New J. Phys.* **2015**, *17*, 083014.
[84] P. Yasaei, B. Kumar, T. Foroozan, C. Wang, M. Asadi, D. Tuschel, J. E. Indacochea, R. F. Klie, A. Salehi-Khojin, *Adv. Mater.* **2015**, *27*, 1887.
[85] Y. Huang, J. Qiao, K. He, S. Bliznakov, E. Sutter, X. Chen, D. Luo, F. Meng, D. Su, J. Decker, W. Ji, R. S. Ruoff, P. Sutter, *Chem. Mater.* **2016**, *28*, 8330.
[86] Z. Zhu, D. Tománek, *Phys. Rev. Lett.* **2014**, *112*, 176802.
[87] J. L. Zhang, S. Zhao, C. Han, Z. Wang, S. Zhong, S. Sun, R. Guo, X. Zhou, C. D. Gu, K. D. Yuan, Z. Li, W. Chen, *Nano Lett.* **2016**, *16*, 4903.
[88] M. Fortin-Deschênes, O. Waller, T. O. Menteş, A. Locatelli, S. Mukherjee, F. Genuzio, P. L. Levesque, A. Hébert, R. Martel, O. Moutanabbir, *Nano Lett.* **2017**, *17*, 4970.
[89] H.-S. Tsai, C.-W. Chen, C.-H. Hsiao, H. Ouyang, J.-H. Liang, *Chem. Commun.* **2016**, *52*, 8409.
[90] B. J. Bowles, *Electrochim. Acta* **1970**, *15*, 737.
[91] Y. Wang, G. Qiu, R. Wang, S. Huang, Q. Wang, Y. Liu, Y. Du, W. A. Goddard, M. J. Kim, X. Xu, P. D. Ye, W. Wu, *Nat. Electron.* **2018**, *1*, 228.
[92] X. Huang, J. Guan, Z. Lin, B. Liu, S. Xing, W. Wang, J. Guo, *Nano Lett.* **2017**, *17*, 4619.
[93] E. J. Weidmann, J. C. Anderson, *Thin Solid Films* **1971**, *7*, 265.
[94] B. M. Huang, T. E. Lister, J. L. Stickney, *Surf. Sci.* **1997**, *392*, 27.
[95] Y. Du, G. Qiu, Y. Wang, M. Si, X. Xu, W. Wu, P. D. Ye, *Nano Lett.* **2017**, *17*, 3965.

[96] Q. Wang, M. Safdar, K. Xu, M. Mirza, Z. Wang, J. He, *ACS Nano* **2014**, *8*, 7497.
[97] Q. Zhong, L. Kong, J. Gou, W. Li, S. Sheng, S. Yang, P. Cheng, H. Li, K. Wu, L. Chen, *Phys. Rev. Mater.* **2017**, *1*, 021001.
[98] C. C. Ren, S. F. Zhang, W. X. Ji, C. W. Zhang, P. Li, P. J. Wang, *Nanomaterials* **2018**, *8*, 698.
[99] D. Wang, L. Chen, X. Wang, G. Cui, P. Zhang, *Phys. Chem. Chem. Phys.* **2015**, *17*, 26979.
[100] J. C. Garcia, D. B. de Lima, L. V. C. Assali, J. F. Justo, *J. Phys. Chem. C* **2011**, *115*, 13242.
[101] D. Wu, S. Wang, J. Yuan, B. Yang, H. Chen, *Phys. Chem. Chem. Phys.* **2017**, *19*, 11771.
[102] H. Sun, S. Mukherjee, C. V. Singh, *Phys. Chem. Chem. Phys.* **2016**, *18*, 26736.
[103] Z. P. Niu, Y. M. Zhang, S. Dong, *New J. Phys.* **2015**, *17*, 073026.
[104] X. Zhang, L. Wei, J. Tan, M. Zhao, *Carbon* **2016**, *105*, 323.
[105] Z. Ni, Q. Liu, K. Tang, J. Zheng, J. Zhou, R. Qin, Z. Gao, D. Yu, J. Lu, *Nano Lett.* **2012**, *12*, 113.
[106] S. Cahangirov, M. Topsakal, E. Aktürk, H. Şahin, S. Ciraci, *Phys. Rev. Lett.* **2009**, *102*, 236804.
[107] X.-L. Yu, L. Huang, J. Wu, *Phys. Rev. B* **2017**, *95*, 125113.
[108] W. Hu, J. Yang, *J. Phys. Chem. C* **2015**, *119*, 20474.
[109] T. Zhao, C. Y. He, S. Y. Ma, K. W. Zhang, X. Y. Peng, G. F. Xie, J. X. Zhong, *J. Phys.: Condens. Matter* **2015**, *27*, 265301.
[110] C. Kamal, M. Ezawa, *Phys. Rev. B* **2015**, *91*, 085423.
[111] S. Mardanya, V. K. Thakur, S. Bhowmick, A. Agarwal, *Phys. Rev. B* **2016**, *94*, 035423.
[112] Y. Xu, B. Peng, H. Zhang, H. Shao, R. Zhang, H. Zhu, *Ann. Phys.* **2017**, *529*, 1600152.
[113] R. R. Q. Freitas, R. Rivelino, F. de Brito Mota, C. M. C. de Castilho, A. Kakanakova-Georgieva, G. K. Gueorguiev, *J. Phys. Chem. C* **2015**, *119*, 23599.
[114] E. Aktürk, O. Ü. Aktürk, S. Ciraci, *Phys. Rev. B* **2016**, *94*, 014115.
[115] H. Liu, Y. Du, Y. Deng, P. D. Ye, *Chem. Soc. Rev.* **2015**, *44*, 2732.
[116] Y. Wang, M. Ye, M. Weng, J. Li, X. Zhang, H. Zhang, Y. Guo, Y. Pan, L. Xiao, J. Liu, F. Pan, J. Lu, *ACS Appl. Mater. Interfaces* **2017**, *9*, 29273.
[117] B. Fu, M. Abid, C.-C. Liu, *New J. Phys.* **2017**, *19*, 103040.
[118] L. Matthes, O. Pulci, F. Bechstedt, *J. Phys.: Condens. Matter* **2013**, *25*, 395305.
[119] T. Amlaki, M. Bokdam, P. J. Kelly, *Phys. Rev. Lett.* **2016**, *116*, 256805.
[120] C. C. Liu, W. Feng, Y. Yao, *Phys. Rev. Lett.* **2011**, *107*, 076802.
[121] S. Jomehpour Zaveh, M. R. Roknabadi, T. Morshedloo, M. Modarresi, *Superlattices Microstruct.* **2016**, *91*, 383.
[122] M. Modarresi, A. Kakoee, Y. Mogulkoc, M. R. Roknabadi, *Comput. Mater. Sci.* **2015**, *101*, 164.
[123] Y. Cai, C.-P. Chuu, C. M. Wei, M. Y. Chou, *Phys. Rev. B* **2013**, *88*, 245408.
[124] W. Xiong, C. Xia, Y. Peng, J. Du, T. Wang, J. Zhang, Y. Jia, *Phys. Chem. Chem. Phys.* **2016**, *18*, 6534.
[125] X.-Q. Wang, H.-D. Li, J.-T. Wang, *Phys. Chem. Chem. Phys.* **2012**, *14*, 3031.
[126] Q. Pang, Y. Zhang, J.-M. Zhang, V. Ji, K.-W. Xu, *Nanoscale* **2011**, *3*, 4330.
[127] D.-X. Xing, C.-C. Ren, S.-F. Zhang, Y. Feng, X.-L. Chen, C.-W. Zhang, P.-J. Wang, *Superlattices Microstruct.* **2017**, *103*, 139.
[128] P. Garg, I. Choudhuri, B. Pathak, *Phys. Chem. Chem. Phys.* **2017**, *19*, 31325.
[129] C. He, X. F. Wang, W. X. Zhang, *Phys. Chem. Chem. Phys.* **2017**, *19*, 18426.
[130] Y. Aierken, O. Leenaerts, F. M. Peeters, *Phys. Chem. Chem. Phys.* **2016**, *18*, 18486.
[131] T. P. Kaloni, U. Schwingenschlögl, *Chem. Phys. Lett.* **2013**, *583*, 137.
[132] M. Yarmohammadi, *Solid State Commun.* **2017**, *250*, 84.
[133] B. Rajbanshi, S. Sarkar, B. Mandal, P. Sarkar, *Carbon* **2016**, *100*, 118.
[134] N. D. Drummond, V. Zólyomi, V. I. Fal'ko, *Phys. Rev. B* **2012**, *85*, 075423.
[135] G. R. Berdiyorov, G. Dixit, M. E. Madjet, *J. Phys.: Condens. Matter* **2016**, *28*, 475001.
[136] X. Li, S. Zhang, F. Q. Wang, Y. Guo, J. Liu, Q. Wang, *Phys. Chem. Chem. Phys.* **2016**, *18*, 14191.
[137] A. Y. Luo, R. Hu, Z. Q. Fan, H. L. Zhang, J. H. Yuan, C. H. Yang, Z. H. Zhang, *Org. Electron.* **2017**, *51*, 277.
[138] P. Garg, I. Choudhuri, A. Mahata, B. Pathak, *Phys. Chem. Chem. Phys.* **2017**, *19*, 3660.
[139] M. D. Brennan, T. Morishita, M. J. S. Spencer, *J. Chem. Phys.* **2016**, *144*, 114704.
[140] R. Quhe, R. Fei, Q. Liu, J. Zheng, H. Li, C. Xu, Z. Ni, Y. Wang, D. Yu, Z. Gao, J. Lu, *Sci. Rep.* **2012**, *2*, 853.
[141] A. A. Kistanov, Y. Cai, K. Zhou, N. Srikanth, S. V. Dmitriev, Y. W. Zhang, *Nanoscale* **2018**, *10*, 1403.
[142] Y.-W. Son, M. L. Cohen, S. G. Louie, *Phys. Rev. Lett.* **2006**, *97*, 216803.
[143] S. Kaneko, H. Tsuchiya, Y. Kamakura, N. Mori, M. Ogawa, *Appl. Phys. Express* **2014**, *7*, 035102.
[144] Z. G. Yu, Y.-W. Zhang, *J. Appl. Phys.* **2015**, *118*, 165706.
[145] N. Gillgren, D. Wickramaratne, Y. Shi, T. Espiritu, J. Yang, J. Hu, J. Wei, X. Liu, Z. Mao, K. Watanabe, *2D Mater.* **2014**, *2*, 011001.
[146] F. Liu, Y. Wang, X. Liu, J. Wang, H. Guo, *IEEE Trans. Electron Devices* **2014**, *61*, 3871.
[147] Y. Liu, F. Xu, Z. Zhang, E. S. Penev, B. I. Yakobson, *Nano Lett.* **2014**, *14*, 6782.
[148] M. Batmunkh, M. Bat-Erdene, G. Shapter Joseph, *Adv. Mater.* **2016**, *28*, 8586.
[149] K. I. Bolotin, K. J. Sikes, Z. Jiang, M. Klima, G. Fudenberg, J. Hone, P. Kim, H. L. Stormer, *Solid State Commun.* **2008**, *146*, 351.
[150] X. Li, J. T. Mullen, Z. Jin, K. M. Borysenko, M. Buongiorno Nardelli, K. W. Kim, *Phys. Rev. B* **2013**, *87*, 115418.
[151] N. J. Roome, J. D. Carey, *ACS Appl. Mater. Interfaces* **2014**, *6*, 7743.
[152] R. W. Dutton, R. S. Muller, *Proc. IEEE* **1971**, *59*, 1511.
[153] D. Akinwande, N. Petrone, J. Hone, *Nat. Commun.* **2014**, *5*, 5678.
[154] Z. Weinan, P. Saungeun, N. Y. Maruthi, A. Deji, *Flexible Printed Electron.* **2017**, *2*, 043001.
[155] W. Zhu, S. Park, M. N. Yogeesh, K. M. McNicholas, S. R. Bank, D. Akinwande, *Nano Lett.* **2016**, *16*, 2301.
[156] C. C. Mayorga-Martinez, Z. Sofer, M. Pumera, *Angew. Chem., Int. Ed.* **2015**, *54*, 14317.
[157] C. Liu, C.-S. Liu, X. Yan, *Phys. Lett. A* **2017**, *381*, 1092.
[158] G. Hu, T. Albrow-Owen, X. Jin, A. Ali, Y. Hu, R. C. T. Howe, K. Shehzad, Z. Yang, X. Zhu, R. I. Woodward, T.-C. Wu, H. Jussila, J.-B. Wu, P. Peng, P.-H. Tan, Z. Sun, E. J. R. Kelleher, M. Zhang, Y. Xu, T. Hasan, *Nat. Commun.* **2017**, *8*, 278.
[159] E. B. Secor, B. Y. Ahn, T. Z. Gao, J. A. Lewis, M. C. Hersam, *Adv. Mater.* **2015**, *27*, 6683.
[160] R. H. Kim, J. Leem, C. Muratore, S. Nam, R. Rao, A. Jawaid, M. Durstock, M. McConney, L. Drummy, R. Rai, A. Voevodin, N. Glavin, *Nanoscale* **2019**, *11*, 13260.
[161] Y. Kim, S. S. Cruz, K. Lee, B. O. Alawode, C. Choi, Y. Song, J. M. Johnson, C. Heidelberger, W. Kong, S. Choi, K. Qiao, I. Almansouri, E. A. Fitzgerald, J. Kong, A. M. Kolpak, J. Hwang, J. Kim, *Nature* **2017**, *544*, 340.
[162] J. Shim, S.-H. Bae, W. Kong, D. Lee, K. Qiao, D. Nezich, Y. J. Park, R. Zhao, S. Sundaram, X. Li, H. Yeon, C. Choi, H. Kum, R. Yue, G. Zhou, Y. Ou, K. Lee, J. Moodera, X. Zhao, J.-H. Ahn, C. Hinkle, A. Ougazzaden, J. Kim, *Science* **2018**, *362*, 665.
[163] N. R. Glavin, K. D. Chabak, E. R. Heller, E. A. Moore, T. A. Prusnick, B. Maruyama, D. E. Walker Jr., D. L. Dorsey, Q. Paduano, M. Snure, *Adv. Mater.* **2017**, *29*, 1701838.
[164] S. Yang, C. Jiang, S.-h. Wei, *Appl. Phys. Rev.* **2017**, *4*, 021304.

[165] X. Liu, T. Ma, N. Pinna, J. Zhang, *Adv. Funct. Mater.* **2017**, *27*, 1702168.
[166] R. Irshad, K. Tahir, B. Li, Z. Sher, J. Ali, S. Nazir, *J. Ind. Eng. Chem.* **2018**, *64*, 60.
[167] L. Kou, T. Frauenheim, C. Chen, *J. Phys. Chem. Lett.* **2014**, *5*, 2675.
[168] S. J. Ray, *Sens. Actuators, B* **2016**, *222*, 492.
[169] A. N. Abbas, B. Liu, L. Chen, Y. Ma, S. Cong, N. Aroonyadet, M. Köpf, T. Nilges, C. Zhou, *ACS Nano* **2015**, *9*, 5618.
[170] S. Cui, H. Pu, S. A. Wells, Z. Wen, S. Mao, J. Chang, M. C. Hersam, J. Chen, *Nat. Commun.* **2015**, *6*, 8632.
[171] X.-P. Chen, L.-M. Wang, X. Sun, R.-S. Meng, J. Xiao, H.-Y. Ye, G.-Q. Zhang, *IEEE Electron Device Lett.* **2017**, *38*, 661.
[172] W. Xia, W. Hu, Z. Li, J. Yang, *Phys. Chem. Chem. Phys.* **2014**, *16*, 22495.
[173] W. Han, *APL Mater.* **2016**, *4*, 032401.
[174] L. Zhang, H. Zhao, W.-X. Ji, C.-W. Zhang, P. Li, P.-J. Wang, *Chem. Phys. Lett.* **2018**, *712*, 78.
[175] Y.-Y. Wang, R.-G. Quhe, D.-P. Yu, J. Lü, *Chin. Phys. B* **2015**, *24*, 087201.
[176] X. Liu, Z. Wei, I. Balla, A. J. Mannix, N. P. Guisinger, E. Luijten, M. C. Hersam, *Sci. Adv.* **2017**, *3*, e1602356.
[177] H. Zhao, Q. Guo, F. Xia, H. Wang, *Nanophotonics* **2015**, *4*, 128.
[178] A. Agarwal, M. S. Vitiello, L. Viti, A. Cupolillo, A. Politano, *Nanoscale* **2018**, *10*, 8938.
[179] Y. Li, Z. Li, C. Chi, H. Shan, L. Zheng, Z. Fang, *Adv. Sci.* **2017**, *4*, 1600430.
[180] F. Xia, H. Wang, D. Xiao, M. Dubey, A. Ramasubramaniam, *Nat. Photonics* **2014**, *8*, 899.
[181] K.-T. Lam, J. Guo, *J. Appl. Phys.* **2015**, *117*, 113105.
[182] Z. Liu, K. Aydin, *Nano Lett.* **2016**, *16*, 3457.
[183] C. Sun, L. Wen, J. Zeng, Y. Wang, Q. Sun, L. Deng, C. Zhao, Z. Li, *Biomaterials* **2016**, *91*, 81.
[184] M. A. Huber, F. Mooshammer, M. Plankl, L. Viti, F. Sandner, L. Z. Kastner, T. Frank, J. Fabian, M. S. Vitiello, T. L. Cocker, *Nat. Nanotechnol.* **2017**, *12*, 207.
[185] G. Konstantatos, *Nat. Commun.* **2018**, *9*, 5266.
[186] F. Xia, T. Mueller, Y.-m. Lin, A. Valdes-Garcia, P. Avouris, *Nat. Nanotechnol.* **2009**, *4*, 839.
[187] M. Casalino, U. Sassi, I. Goykhman, A. Eiden, E. Lidorikis, S. Milana, D. De Fazio, F. Tomarchio, M. Iodice, G. Coppola, A. C. Ferrari, *ACS Nano* **2017**, *11*, 10955.
[188] F. Gong, F. Wu, M. Long, F. Chen, M. Su, Z. Yang, J. Shi, *Phys. Status Solidi RRL* **2018**, *12*, 1800310.
[189] M. Huang, M. Wang, C. Chen, Z. Ma, X. Li, J. Han, Y. Wu, *Adv. Mater.* **2016**, *28*, 3481.
[190] M. Buscema, D. J. Groenendijk, S. I. Blanter, G. A. Steele, H. S. van der Zant, A. Castellanos-Gomez, *Nano Lett.* **2014**, *14*, 3347.
[191] M. Amani, C. Tan, G. Zhang, C. Zhao, J. Bullock, X. Song, H. Kim, V. R. Shrestha, Y. Gao, K. B. Crozier, M. Scott, A. Javey, *ACS Nano* **2018**, *12*, 7253.
[192] B. Guo, S.-H. Wang, Z.-X. Wu, Z.-X. Wang, D.-H. Wang, H. Huang, F. Zhang, Y.-Q. Ge, H. Zhang, *Opt. Express* **2018**, *26*, 22750.
[193] J. Wu, G. K. W. Koon, D. Xiang, C. Han, C. T. Toh, E. S. Kulkarni, I. Verzhbitskiy, A. Carvalho, A. S. Rodin, S. P. Koenig, *ACS Nano* **2015**, *9*, 8070.
[194] L. Zeng, L. Tao, C. Tang, B. Zhou, H. Long, Y. Chai, S. P. Lau, Y. H. Tsang, *Sci. Rep.* **2016**, *6*, 20343.
[195] T. Wang, K. Andrews, A. Bowman, T. Hong, M. Koehler, J. Yan, D. Mandrus, Z. Zhou, Y.-Q. Xu, *Nano Lett.* **2018**, *18*, 2766.
[196] X. Wang, P. Wang, J. Wang, W. Hu, X. Zhou, N. Guo, H. Huang, S. Sun, H. Shen, T. Lin, *Adv. Mater.* **2015**, *27*, 6575.
[197] Z. Sun, T. Hasan, F. Torrisi, D. Popa, G. Privitera, F. Wang, F. Bonaccorso, D. M. Basko, A. C. Ferrari, *ACS Nano* **2010**, *4*, 803.
[198] Y. Chen, G. Jiang, S. Chen, Z. Guo, X. Yu, C. Zhao, H. Zhang, Q. Bao, S. Wen, D. Tang, D. Fan, *Opt. Express* **2015**, *23*, 12823.
[199] J. Li, H. Luo, B. Zhai, R. Lu, Z. Guo, H. Zhang, Y. Liu, *Sci. Rep.* **2016**, *6*, 30361.
[200] X. M. Liu, H. R. Yang, Y. D. Cui, G. W. Chen, Y. Yang, X. Q. Wu, X. K. Yao, D. D. Han, X. X. Han, C. Zeng, J. Guo, W. L. Li, G. Cheng, L. M. Tong, *Sci. Rep.* **2016**, *6*, 26024.
[201] G. Wang, Y. Zhang, C. You, B. Liu, Y. Yang, H. Li, A. Cui, D. Liu, H. Yan, *Infrared Phys. Technol.* **2018**, *88*, 149.
[202] F. Wang, Z. Wang, L. Yin, R. Cheng, J. Wang, Y. Wen, T. A. Shifa, F. Wang, Y. Zhang, X. Zhan, J. He, *Chem. Soc. Rev.* **2018**, *47*, 6296.
[203] M. Buscema, J. O. Island, D. J. Groenendijk, S. I. Blanter, G. A. Steele, H. S. J. van der Zant, A. Castellanos-Gomez, *Chem. Soc. Rev.* **2015**, *44*, 3691.
[204] Q. Guo, A. Pospischil, M. Bhuiyan, H. Jiang, H. Tian, D. Farmer, B. Deng, C. Li, S.-J. Han, H. Wang, Q. Xia, T.-P. Ma, T. Mueller, F. Xia, *Nano Lett.* **2016**, *16*, 4648.
[205] X. Chen, X. Lu, B. Deng, O. Sinai, Y. Shao, C. Li, S. Yuan, V. Tran, K. Watanabe, T. Taniguchi, D. Naveh, L. Yang, F. Xia, *Nat. Commun.* **2017**, *8*, 1672.
[206] M. Buscema, D. J. Groenendijk, G. A. Steele, H. S. J. van der Zant, A. Castellanos-Gomez, *Nat. Commun.* **2014**, *5*, 4651.
[207] H. Fang, W. Hu, *Adv. Sci.* **2017**, *4*, 1700323.
[208] U. Keller, *Nature* **2003**, *424*, 831.
[209] A. Martinez, Z. Sun, *Nat. Photonics* **2013**, *7*, 842.
[210] J. He, L. Tao, H. Zhang, B. Zhou, J. Li, *Nanoscale* **2019**, *11*, 2577.
[211] R. Woodward, E. Kelleher, *Appl. Sci.* **2015**, *5*, 1440.
[212] Z. Sun, A. Martinez, F. Wang, *Nat. Photonics* **2016**, *10*, 227.
[213] Z. Luo, D. Wu, B. Xu, H. Xu, Z. Cai, J. Peng, J. Weng, S. Xu, C. Zhu, F. Wang, *Nanoscale* **2016**, *8*, 1066.
[214] J. Sotor, G. Sobon, W. Macherzynski, P. Paletko, K. M. Abramski, *Appl. Phys. Lett.* **2015**, *107*, 051108.
[215] Z. Qin, G. Xie, H. Zhang, C. Zhao, P. Yuan, S. Wen, L. Qian, *Opt. Express* **2015**, *23*, 24713.
[216] D. Li, H. Jussila, L. Karvonen, G. Ye, H. Lipsanen, X. Chen, Z. Sun, *Sci. Rep.* **2015**, *5*, 15899.
[217] J. Ma, S. Lu, Z. Guo, X. Xu, H. Zhang, D. Tang, D. Fan, *Opt. Express* **2015**, *23*, 22643.
[218] L. Kong, Z. Qin, G. Xie, Z. Guo, H. Zhang, P. Yuan, L. Qian, *Laser Phys. Lett.* **2016**, *13*, 045801.
[219] S. B. Lu, L. L. Miao, Z. N. Guo, X. Qi, C. J. Zhao, H. Zhang, S. C. Wen, D. Y. Tang, D. Y. Fan, *Opt. Express* **2015**, *23*, 11183.
[220] J. Sotor, G. Sobon, M. Kowalczyk, W. Macherzynski, P. Paletko, K. M. Abramski, *Opt. Lett.* **2015**, *40*, 3885.
[221] M. Zhang, Q. Wu, F. Zhang, L. Chen, X. Jin, Y. Hu, Z. Zheng, H. Zhang, *Adv. Opt. Mater.* **2019**, *7*, 1800224.
[222] D. Na, K. Park, K.-H. Park, Y.-W. Song, *Nanotechnology* **2017**, *28*, 475207.
[223] C. Wang, L. Wang, X. Li, W. Luo, T. Feng, Y. Zhang, P. Guo, Y. Ge, *Nanotechnology* **2019**, *30*, 025204.
[224] L. Lu, Z. Liang, L. Wu, Y. Chen, Y. Song, S. C. Dhanabalan, J. S. Ponraj, B. Dong, Y. Xiang, F. Xing, *Laser Photonics Rev.* **2018**, *12*, 1700221.
[225] M. Wang, F. Zhang, Z. Wang, Z. Wu, X. Xu, *Opt. Express* **2018**, *26*, 4085.
[226] W. Li, Y. Yang, G. Zhang, Y.-W. Zhang, *Nano Lett.* **2015**, *15*, 1691.
[227] H. R. Jiang, Z. Lu, M. C. Wu, F. Ciucci, T. S. Zhao, *Nano Energy* **2016**, *23*, 97.
[228] B. Xiao, Y. C. Li, X. F. Yu, J. B. Cheng, *ACS Appl. Mater. Interfaces* **2016**, *8*, 35342.
[229] J. Zhuang, X. Xu, G. Peleckis, W. Hao, S. X. Dou, Y. Du, *Adv. Mater.* **2017**, *29*, 1606716.
[230] C. Zhang, M. Yu, G. Anderson, R. R. Dharmasena, G. Sumanasekera, *Nanotechnology* **2017**, *28*, 075401.

[231] B. Mortazavi, A. Dianat, G. Cuniberti, T. Rabczuk, *Electrochim. Acta* **2016**, *213*, 865.
[232] H. Benzidi, M. Lakhal, M. Garara, A. Benyoussef, M. Hamedoun, A. El kenz, O. Mounkachi, *J. Mater. Sci. Eng.* **2018**, *7*, 81.
[233] A. Sengupta, T. Frauenheim, *Mater. Today Energy* **2017**, *5*, 347.
[234] G. Wang, X. Shen, J. Yao, J. Park, *Carbon* **2009**, *47*, 2049.
[235] X. Feng, G. Binghui, C. Jing, N. Arokia, L. X. Linhuo, M. Hongyu, M. Huihua, Z. Chongyang, X. Weiwei, L. Zhengrui, L. Shengli, Y. Kaihao, W. Lijun, C. Yiping, S. Litao, Z. Yimei, *2D Mater.* **2016**, *3*, 035021.
[236] Y. R. Lim, F. Shojaei, K. Park, C. S. Jung, J. Park, W. I. Cho, H. S. Kang, *Nanoscale* **2018**, *10*, 7047.
[237] A. Manthiram, Y. Fu, S.-H. Chung, C. Zu, Y.-S. Su, *Chem. Rev.* **2014**, *114*, 11751.
[238] A. Manthiram, Y. Fu, Y.-S. Su, *Acc. Chem. Res.* **2013**, *46*, 1125.
[239] L. Li, L. Chen, S. Mukherjee, J. Gao, H. Sun, Z. Liu, X. Ma, T. Gupta, V. Singh Chandra, W. Ren, H.-M. Cheng, N. Koratkar, *Adv. Mater.* **2017**, *29*, 1602734.
[240] C. Vaalma, D. Buccholz, M. Weil, S. Passerini, *Nat. Rev. Mater.* **2018**, *3*, 18013.
[241] J. He, Y. Wei, T. Zhai, H. Li, *Mater. Chem. Front.* **2018**, *2*, 437.
[242] V. V. Kulish, O. I. Malyi, C. Persson, P. Wu, *Phys. Chem. Chem. Phys.* **2015**, *17*, 13921.
[243] D. Su, S. Dou, G. Wang, *Nano Energy* **2015**, *12*, 88.
[244] W. Tian, S. Zhang, C. Huo, D. Zhu, Q. Li, L. Wang, X. Ren, L. Xie, S. Guo, P. K. Chu, H. Zeng, K. Huo, *ACS Nano* **2018**, *12*, 1887.
[245] Y. Liu, X. Peng, *Appl. Mater. Today* **2017**, *8*, 104.
[246] Y. Han, Y. Ge, Y. Chao, C. Wang, G. G. Wallace, *J. Energy Chem.* **2018**, *27*, 57.
[247] S. Mukherjee, Z. Ren, G. Singh, *Nano-Micro Lett.* **2018**, *10*, 70.
[248] C. Hao, B. Yang, F. Wen, J. Xiang, L. Li, W. Wang, Z. Zeng, B. Xu, Z. Zhao, Z. Liu, *Adv. Mater.* **2016**, *28*, 3194.
[249] X. Chen, G. Xu, X. Ren, Z. Li, X. Qi, K. Huang, H. Zhang, Z. Huang, J. Zhong, *J. Mater. Chem. A* **2017**, *5*, 6581.
[250] H. Xiao, Z.-S. Wu, L. Chen, F. Zhou, S. Zheng, W. Ren, H.-M. Cheng, X. Bao, *ACS Nano* **2017**, *11*, 7284.
[251] S. Luo, J. Zhao, J. Zou, Z. He, C. Xu, F. Liu, Y. Huang, L. Dong, L. Wang, H. Zhang, *ACS Appl. Mater. Interfaces* **2018**, *10*, 3538.
[252] E. Martínez-Periñán, P. Down Michael, C. Gibaja, E. Lorenzo, F. Zamora, E. Banks Craig, *Adv. Energy Mater.* **2018**, *8*, 1702606.
[253] E. Paek, A. J. Pak, K. E. Kweon, G. S. Hwang, *J. Phys. Chem. C* **2013**, *117*, 5610.
[254] E. Paek, A. J. Pak, G. S. Hwang, *J. Electrochem. Soc.* **2013**, *160*, A1.
[255] G. M. Yang, Q. Xu, X. Fan, W. T. Zheng, *J. Phys. Chem. C* **2018**, *122*, 1903.
[256] Y. Wu, C. Cao, *Sci. China Mater.* **2018**, *61*, 1517.
[257] L. D. Hicks, M. S. Dresselhaus, *Phys. Rev. B* **1993**, *47*, 16631.
[258] L. D. Hicks, M. S. Dresselhaus, *Phys. Rev. B* **1993**, *47*, 12727.
[259] P. Puneet, R. Podila, M. Karakaya, S. Zhu, J. He, T. M. Tritt, M. S. Dresselhaus, A. M. Rao, *Sci. Rep.* **2013**, *3*, 3212.
[260] F. Liu, L. Hu, M. Karakaya, P. Puneet, R. Rao, R. Podila, S. Bhattacharya, A. M. Rao, *Sci. Rep.* **2017**, *7*, 16535.
[261] K.-X. Chen, S.-S. Lyu, X.-M. Wang, Y.-X. Fu, Y. Heng, D.-C. Mo, *J. Phys. Chem. C* **2017**, *121*, 13035.
[262] J. Carrete, L. J. Gallego, N. Mingo, *J. Phys. Chem. Lett.* **2017**, *8*, 1375.
[263] Z.-Y. Ong, Y. Cai, G. Zhang, Y.-W. Zhang, *J. Phys. Chem. C* **2014**, *118*, 25272.
[264] L.-D. Zhao, S.-H. Lo, Y. Zhang, H. Sun, G. Tan, C. Uher, C. Wolverton, V. P. Dravid, M. G. Kanatzidis, *Nature* **2014**, *508*, 373.
[265] F. Liu, P. Parajuli, R. Rao, P. C. Wei, A. Karunarathne, S. Bhattacharya, R. Podila, J. He, B. Maruyama, G. Priyadarshan, J. R. Gladden, Y. Y. Chen, A. M. Rao, *Phys. Rev. B* **2018**, *98*, 224309.
[266] S. Wang, W. Wang, G. Zhao, *Phys. Chem. Chem. Phys.* **2016**, *18*, 31217.
[267] G. Qin, Q.-B. Yan, Z. Qin, S.-Y. Yue, M. Hu, G. Su, *Phys. Chem. Chem. Phys.* **2015**, *17*, 4854.
[268] Z. Tian, S. Lee, G. Chen, *J. Heat Transfer* **2013**, *135*, 061605.
[269] R. Fei, A. Faghaninia, R. Soklaski, J.-A. Yan, C. Lo, L. Yang, *Nano Lett.* **2014**, *14*, 6393.
[270] Y. Sun, D. Wang, Z. Shuai, *J. Phys. Chem. C* **2017**, *121*, 19080.
[271] L. Cheng, H. Liu, X. Tan, J. Zhang, J. Wei, H. Lv, J. Shi, X. Tang, *J. Phys. Chem. C* **2014**, *118*, 904.

